Review

Iron core mineralisation in prokaryotic ferritins

Nick E. Le Brun [a,*], Allister Crow [a,1], Michael E.P. Murphy [b], A. Grant Mauk [c], Geoffrey R. Moore [a]

[a] Centre for Molecular and Structural Biochemistry, School of Chemistry, University of East Anglia, Norwich, NR4 7TJ, UK
[b] Department of Microbiology and Immunology, University of British Columbia, Vancouver, British Columbia, Canada V6T 1Z3
[c] Department of Biochemistry and Molecular Biology, University of British Columbia, Vancouver, British Columbia, Canada V6T 1Z3

ARTICLE INFO

ABSTRACT

Background: To satisfy their requirement for iron while at the same time countering the toxicity of this highly reactive metal ion, prokaryotes have evolved proteins belonging to two distinct sub-families of the ferritin family: the bacterioferritins (BFRs) and the bacterial ferritins (Ftns). Recently, Ftn homologues have also been identified and characterised in archaeon species. All of these prokaryotic ferritins function by solubilising and storing large amounts of iron in the form of a safe but bio-available mineral.
Scope of review: The mechanism(s) by which the iron mineral is formed by these proteins is the subject of much current interest. Here we review the available information on these proteins, with particular emphasis on significant advances resulting from recent structural, spectroscopic and kinetic studies.
Major conclusions: Current understanding indicates that at least two distinct mechanisms are in operation in prokaryotic ferritins. In one, the ferroxidase centre acts as a true catalytic centre in driving Fe^{2+} oxidation in the cavity; in the other, the centre acts as a gated iron pore by oxidising Fe^{2+} and transferring the resulting Fe^{3+} into the central cavity.
General significance: The prokaryotic ferritins exhibit a wide variation in mechanisms of iron core mineralisation. The basis of these differences lies, at least in part, in structural differences at and around the catalytic centre. However, it appears that more subtle differences must also be important in controlling the iron chemistry of these remarkable proteins.

© 2010 Elsevier B.V. All rights reserved.

1. The chemistry and biology of iron

Iron most commonly occurs in either the $+2$ and $+3$ oxidation states and can readily cycle between them. This ability underpins its importance in many diverse biochemical processes, but also means that it is potentially extremely toxic. The $+2$ state is more thermodynamically stable ($E^{o}Fe^{3+}/Fe^{2+} = +0.77$ V versus NHE), but is readily oxidised to Fe^{3+} by dioxygen ($E^{o}O_2/H_2O = +1.23$ V versus NHE) and other reactive oxygen species, generating reduced oxygen species such as superoxide, hydrogen peroxide and water. Hydrogen peroxide, which is a by-product of aerobic respiration, readily reacts with Fe^{2+} in a reaction known as the Fenton reaction [1], to generate the extremely reactive and, therefore, toxic, hydroxyl radical, OH. This will react on collision with all types of biological macromolecules, usually perturbing their activity and sometimes inactivating them completely. Fe^{3+} can be reduced back to Fe^{2+} by a number of cytoplasmic reductants, including low molecular weight thiols and superoxide, resulting in a destructive

catalytic cycle known as the Haber–Weiss reaction. Recently it has been suggested that this chemistry underpins a broad range of antibiotics [2].

The propensity of Fe^{2+} to react with dioxygen to generate Fe^{3+} is the basis of another significant problem for biology because Fe^{3+} is highly insoluble; it precipitates as the uncharged species $Fe(OH)_3(H_2O)_3$ (K_{sp}, of $\sim 10^{-38}$) [1], thereby limiting the concentration of $Fe(OH_2)_6^{3+}$ at neutral pH 7 to $\sim 10^{-17}$ M. Thus, under aerobic conditions and at physiological pH, its bioavailability is commonly extremely poor, such that it is often a limiting nutrient for growth and for virulence in bacterial pathogens [3]. Faced with the difficulties imposed by iron chemistry, organisms have evolved mechanisms to both acquire and maintain iron in a non-toxic form. The latter is achieved through storage of iron as a ferric oxyhydroxide mineral solubilised within members of the ferritin family of proteins [4–6].

2. Ferritins—nature's solution to the iron problem

Oligomeric proteins composed of subunits that assemble to form an essentially spherical shell are capable of storing iron. The first family of iron storage proteins to be discovered were the vertebrate ferritins, which consist of 24 α-helical subunits of $M_w \sim 20$ kDa that assemble to form a roughly spherical hollow shell with an outer diameter of ~ 120 Å and an inner diameter of ~ 80 Å [4,6,7]. Vertebrate ferritins catalyse the oxidation of Fe^{2+} to Fe^{3+} and promote the formation of an iron

* Corresponding author. School of Chemistry, University of East Anglia, Norwich, NR4 7TJ, UK. Tel.: +44 1603 592699; fax: +44 1603 592003.
E-mail address: n.le-brun@uea.ac.uk (N.E. Le Brun).
[1] Current address: Department of Biological Chemistry, John Innes Centre, Norwich Research Park, Colney, Norwich NR4 7UH, UK.
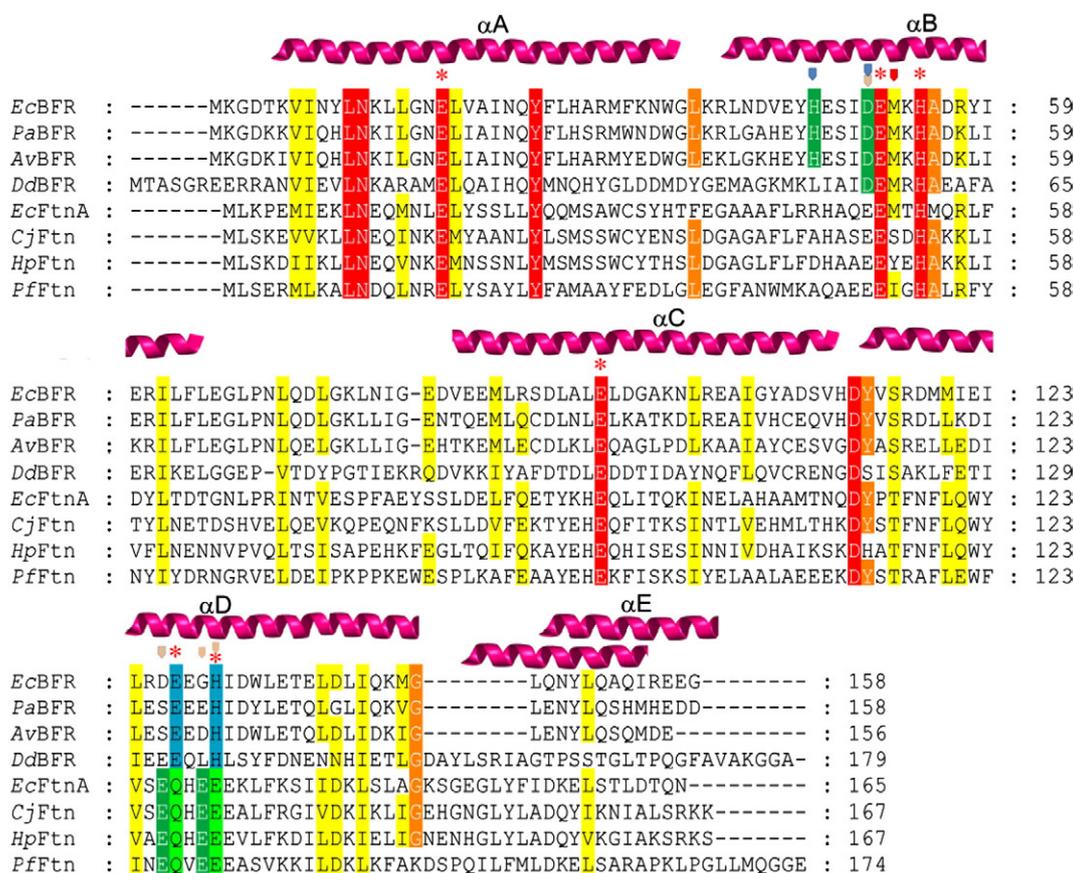
oxyhydroxide mineral within their central cavity. Mammalian ferritins are composed of two different subunit types, H and L, which have 55% amino acid residue identity and are isostructural, meaning that they can assemble in any proportion in the 24mer, and different tissues contain ferritins with different subunit compositions [8]. The most important difference between these subunits is that the catalytic centre, known as the ferroxidase centre, that is particularly important for the early stages of core mineralisation is found only in the H-chain subunit. Ferritins are found in all types of organisms from mammals to bacteria, and while there is relatively low overall sequence conservation, the three-dimensional structure and symmetry of the oligomer is remarkably highly conserved. Nevertheless, significant structural variations do exist and, as discussed below, these lead to mechanistic diversity. A second family of proteins that have the ability to store iron, the DNA binding protein from starved cells (Dps) family, was discovered relatively recently [9,10]. These are also oligomeric proteins and have a α-helical subunit structure related to that of ferritins, and are sometimes referred to as being ferritin proteins; however, they assemble into 12mers and have quite different catalytic sites and iron mineralisation characteristics. These are described in detail in this issue [11] and, therefore, will not be covered in any detail here.

2.1. Types of prokaryotic ferritins

Two different types of ferritins are found in bacteria, often within the same cell. These are the bacterioferritins (BFRs) and the bacterial ferritins (Ftns). Recently, Ftn homologues have been discovered and characterised in the archaea [12,13]. The rather subtle nomenclature reflects that the proteins have significant similarities but also important differences, as discussed below. An amino acid residue sequence alignment of BFR and Ftn proteins reveals that, outside of catalytically important residues (see below), rather few residues are conserved between the two ferritin sub-families (Fig. 1), with sequence identities between pairs of sequences generally <15%. A more comprehensive review of the evolutionary relationship between BFRs and Ftns, and other members of the ferritin family is provided in this issue [14].

Both types of ferritin play a role in iron storage, but may also have more specialised functions in iron metabolism or in iron detoxification. The precise roles of the proteins vary depending on the particular organism. For example, in *Escherichia coli*, a bacterial ferritin functions as the principal iron store [15], while in *Salmonella enterica* sv. typhimurium, BFR is the major iron storage protein [16]. In the pathogen *Erwinia chrysanthemi*, BFR is not the principal iron store but instead is functionally connected to the Suf iron-sulfur cluster biosynthetic apparatus [17]. In *Helicobacter pylori*, Ftn is essential for host colonisation [18]. In some cases, the proteins appear to have dual roles; for example, in *Bacteroides fragilis* and *Campylobacter jejuni*, the ferritin FtnA is involved in iron storage and redox stress response [19,20] and in the cyanobacterium *Synechocystis* sp. PCC 6803 and *Neisseria gonorrhoeae*, BFR appears to have a similar dual role [21,22]. More information is required about the physiological roles of prokaryotic ferritins, and in particular about the interplay between ferritins and the diversity of their roles where they co-exist in the same cell.

Fig. 1. Amino acid residue sequence alignment of BFR and Ftn proteins. Protein sequences correspond to *E. coli* BFR (*Ec*BFR), *Pseudomonas aeruginosa* BFR (*Pa*BFR), *Azotobacter vinelandii* BFR (*Av*BFR), *Desulfovibrio desulfuricans* BFR (*Dd*BFR), *E. coli* FtnA (*Ec*FtnA), *Campylobacter jejuni* Ftn (*Cj*Ftn), *Helicobacter pylori* Ftn (*Hp*Ftn) and *Pyrococcus furiosis* Ftn (*Pf*Ftn). The alignment was performed using ClustalW [111] and the figure generated using Genedoc [112]. Residue numbers are indicated on the right. The positions of the five helices of the ferritin subunit are represented as cartoon helices above the alignment. The fifth helix (αE) is indicated in two positions due to a gap in the alignment for three of the BFR proteins (the upper helix corresponds to *Ec*BFR, *Pa*BFR and *Av*BFR, while the lower helix corresponds to *Dd*BFR, *Ec*FtnA, *Cj*Ftn, *Hp*Ftn and *Pf*Ftn. Asterisks indicate residues that serve as ligands at the ferroxidase centre of BFR and Ftn. Blue arrows indicate the position of residues that coordinate iron at the inner surface site of BFR, while beige arrows indicate residues that coordinate iron at site C of Ftn proteins (see main text for details). A red arrow indicates the Met residue that serves as the heme ligand in BFRs.
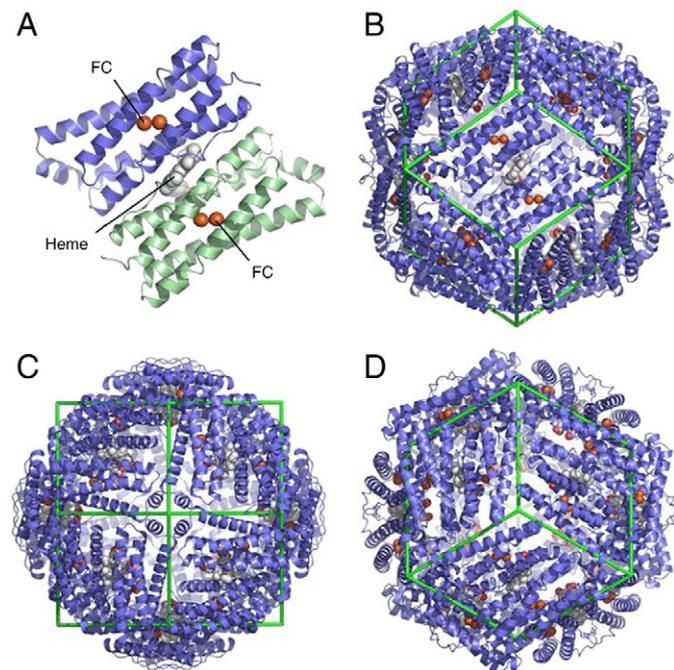
2.1.1. Bacterioferritins

The first ferritin to be unambiguously identified in bacteria was the bacterioferritin (BFR) of *Azotobacter vinlandii* [23], and since then BFRs have been isolated from a wide variety of bacteria, including *E. coli*, *Rhodobacter capsulatus* and *Desulfovibrio desulfuricans* [24,25]. Amongst the ferritins, BFRs are unique in that they contain heme (discussed further in Section 3.1). The BFR subunit is composed of a four α-helical bundle with a fifth, short helix at the C-terminal. A long loop connects helices B and C such that helices B and C are parallel. 24 such subunits are arranged in a highly symmetric fashion, with a dimer of subunits forming each face of a dodecahedron, with 4,3,2 symmetry, see Fig. 2 [26–32]. BFRs are in most cases homopolymers. Some bacteria, for example, *Pseudomonas aeruginosa*, *P. putida* and the cyanobacterium *Synechocystis*, encode two BFR subunits, but even in these cases, it is not clear whether these co-assemble into heteropolymers [33–35]. All BFR subunits are of the H-chain-type; they are not particularly similar to eukaryotic H-chain ferritins in terms of overall sequence similarity (~20% identity), but conserved within them are some of the key residues that constitute the catalytic ferroxidase centre, see Section 3.2.1 below.

The symmetric arrangement of subunits in ferritins gives rise to a number of different channels through the protein coat, connecting the protein cavity with the external solution. Thus BFR contains eight channels at the three-fold and six channels at the four-fold symmetry axes, see Fig. 3A and B. Both types of channels are hydrophilic in character in BFR, while in eukaryotic ferritins, the three-fold channels are hydrophilic but the four-fold channels are hydrophobic, with little or no conservation of residues in these regions. In addition to these, there is a further type of channel, termed B-channels, which occur where one subunit dimer meets another in a side-on fashion, such that there are 12 such channels per BFR (Fig. 3C) [28,36]. Exchange of metal ions, protons and anions between the cavity and external solution occurs during mineralisation (and iron release), but the roles of each of the channels in this are not yet clear.

2.1.2. Bacterial ferritins

In the early '90s another type of ferritin was discovered in *E. coli* and was named bacterial ferritin (FtnA) [37]. Homologues have been subsequently identified in many other bacteria, including *Campylobacter jejuni*, *Porphyromonas gingivalis* and *H. pylori* [18,38,39]. Ftn proteins, which share only ~10 – 15% identity with BFRs (Fig. 1), generally consist of 24 H-chain-like subunits (Fig. 4A) arranged as dodecahedron with 4,3,2 symmetry (Fig. 4B). A second type of Ftn, called FtnB, which does not contain a typical catalytic centre has also been identified in *E. coli* and in *Salmonella enterica* sv. typhimurium. In the latter, *in vivo* studies indicated a role for this bacterial ferritin in iron-sulfur cluster repair and virulence [16]. As with BFR, in species that encode more than one Ftn protein subunit heteropolymers may exist but have not been identified. *E. coli* FtnA is the best studied bacterial ferritin [15,40–43]. Although only distantly related to eukaryotic H-chain ferritin, in terms of sequence (~22% identity), it bears a striking structural similarity to human H-chain, and, therefore, possesses eight three-fold and six four-fold channels. The three-fold channels are lined by both hydrophobic and hydrophilic residues and are significantly less polar than their eukaryotic ferritin equivalents. The four-fold channels are polar at both ends and hydrophobic in character in their central part. B-channels are also present in Ftns (but not in eukaryotic ferritins) [28]. One possibility is that B-channels in BFRs and Ftns are functionally equivalent to eukaryotic ferritin three-fold channels. The structures of a number of other bacterial Ftn proteins have been solved, including those of *Campylobacter jejuni* [38] and *Helicobacter pylori* [44], and both of these proteins bear a high degree of structural similarity to *E. coli* FtnA.
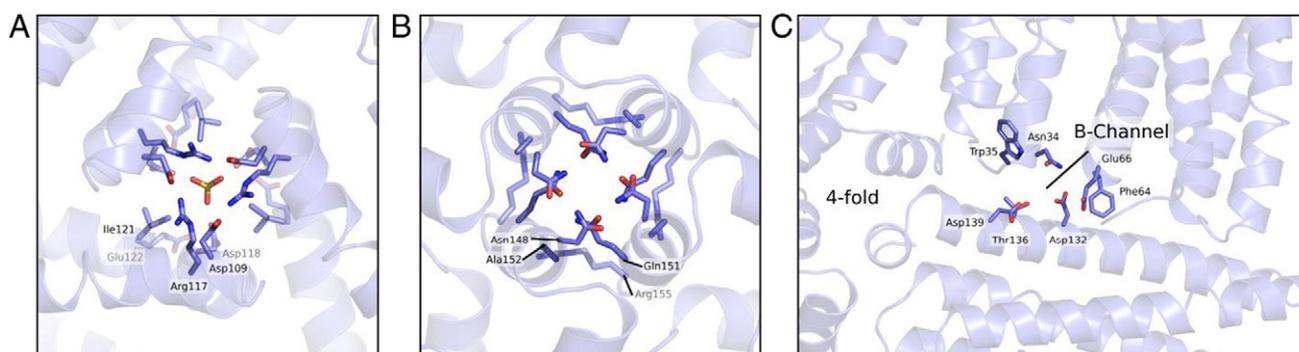
2.1.3. Archaeal ferritins

Ftn proteins from two archaea have recently been structurally characterised. The first was from the hyperthermophilic archaeon *Archaeoglobus fulgidis*, which is 37% identical to *E. coli* FtnA [12]. This revealed a typical ferritin subunit structure, but a quite different quaternary arrangement, with 3,2 tetrahedral symmetry instead of the 4,3,2 octahedral symmetry of other 24meric ferritins (although it is noted that such symmetry is found in the 12mer Dps proteins), see Fig. 4C. The result of this is that, although the protein shell is roughly spherical, it is less densely packed with slightly larger overall dimensions, and there are four super-pores of 45 Å diameter connecting the cavity with the outside environment. The pores are hydrophilic and carry a net positive charge. In the absence of an iron core, the protein was found to dissociate into subunit dimers; the 24meric structure was stabilised by the iron core. The difference in symmetry appears to be due to amino acid residue differences in the region of the fifth, E-helix that prevent association of subunits with four-fold symmetry. This novel structural arrangement is not, however, a common feature amongst archaeon Ftn proteins. The structure of *Pyrococcus furiosis* Ftn (which is 51% identical to the *A. fulgidis* Ftn) exhibits the classic ferritin 4,3,2 symmetry, with three- and four-fold channels with similar properties to those of *E. coli* FtnA [13]. B-type channels are also found in archaeal Ftn proteins, but, as with other ferritins, the precise function of each of the channels has not been clearly established.

3. Iron centres of prokaryotic ferritins

3.1. The heme group of BFR

BFR uniquely contains up to 12 heme groups per 24mer [23,26], though overproduction of the polypeptide chain usually results in a heme loading lower than 12. *D. desulfuricans* BFR is unusual in that it contains iron-coproporphyrin III, rather than iron-protoporphyrin IX [28]. The hemes are located at 2-fold symmetric inter-subunit sites, where they are ligated to the protein by two methionine residues (located in adjacent subunits) [45,46], see Figs. 1 and 5. Bis-thioether axial coordination of heme is highly unusual. To our knowledge, only one other example of this has been reported, in the streptococcal cell surface protein Shp, which is involved in heme acquisition and uptake [47]. The ligand field generated by bis-methionine coordination is sufficient to make the heme iron low

Fig. 2. Structure of BFR. Cartoon representations of A, the *E. coli* BFR (pdb 3E1M) subunit dimer peptide backbone showing the position of the intra-subunit dinuclear ferroxidase centre and inter-subunit heme site, B–D, the overall structure of 24meric *E. coli* BFR looking down a two-fold (B), four-fold (C) and three-fold (D) symmetry axis. This and other structural figures were prepared using Pymol [113].

Fig. 3. Trans-protein channels connecting the inner cavity of BFR with the environment. Cartoon representations of the A, three-fold, B, four fold, and C, B-channels of *E. coli* BFR. In A, a sulfate ion is bound in the channel, while in C a closely lying four-fold channel is located to the left of the B-channel in the view shown. Similar channels are found in bacterial ferritins (Ftn proteins).
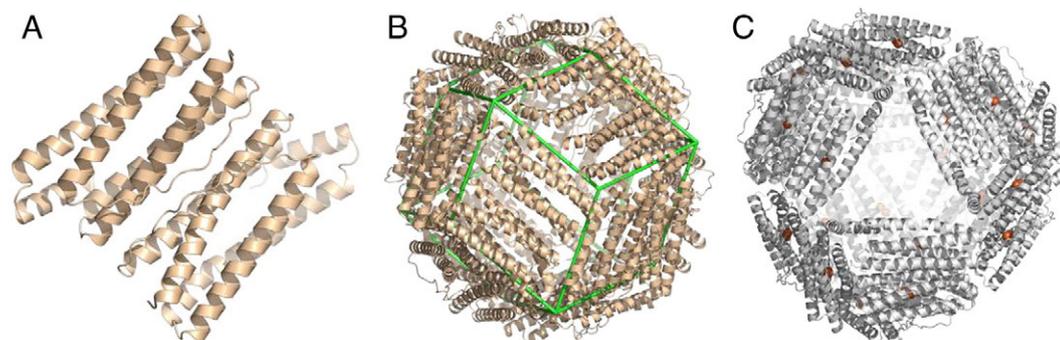
spin (in both Fe^{2+} and Fe^{3+} forms). It has been shown that the hemes do not play a role in the aerobic oxidative uptake of Fe^{2+}, as substitution of the heme coordinating Met52 in *E. coli* BFR, resulting in a heme-free variant, did not affect mineralisation properties [48]. Significantly increased iron loadings in as isolated heme-free BFR led to the suggestion that heme plays an important role in iron release [48]. Evidence in support of this proposal is now beginning to emerge; a study of *P. aeruginosa* BFR reported that heme reduction was associated with efficient iron mobilisation [49].
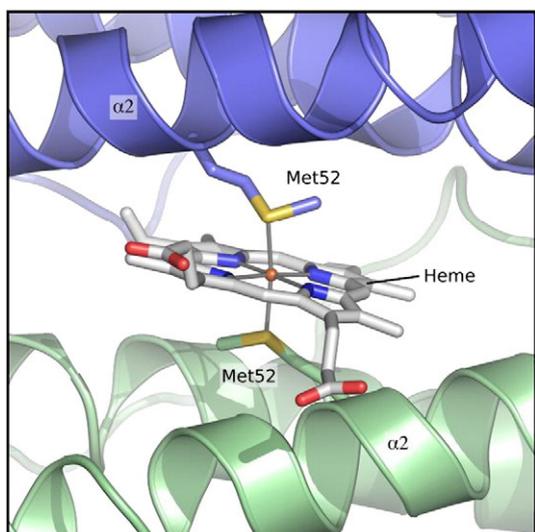
3.2. The ferroxidase centre

The ferroxidase centre of eukaryotic H-chain ferritins has been intensively studied for several decades, but due to instability of the iron-bound form, a structure of the ferroxidase centre in an iron-bound form is not yet available. Nevertheless, structural data on forms of the protein containing other divalent metal ions has enabled a detailed model of the centre to be constructed [50–52]. For the purposes of comparison with prokaryotic ferroxidase centres, it is useful to review here briefly the details of the H-chain centre. The centre consists of two iron sites, FeA and FeB, in which FeA is ligated by a histidine (His65, human H-chain numbering), a monodentate glutamate (Glu27) and a bridging glutamate (Glu62), while FeB is ligated by Glu62 and two monodentate glutamates (Glu61 and Glu107), see Fig. 6A. Structural data of ferritin containing Tb^{3+} at the centre rather than Fe^{3+} [53] revealed that Glu61 is able to adopt two conformations: one bound to the metal at the B site and in the other projecting towards the cavity, leading to the suggestion that this ligand might play a role in iron transfer into the cavity. However, more recent structures of H-chain ferritins containing Zn^{2+} [52] and Zn^{2+} or Mn^{2+} [54], did not feature Glu61 as a ligand to FeB. In addition to these directly coordinating residues, Tyr34 and Gln141 formed hydrogen bonds to Glu107 and a water molecule was ligated to FeA. In the sections below, the ferroxidase centres of prokaryotic ferritins are discussed in detail, revealing significant structural differences with the H-chain centre.

3.2.1. The BFR ferroxidase centre

BFRs contain an intra-subunit ferroxidase centre that is similar to, but distinct from, that of H-chain ferritin. Like H-chain ferritin, the centre is a dinuclear iron site, see Figs. 6B, 7A and C, which show the di-Fe^{2+} form of the centre [55]. Fe1 and Fe2 are both ligated by terminal glutamate (Glu18/Glu94 for Fe1 and Fe2, respectively, *E. coli* BFR numbering, Fig. 1) and histidine (His54/His130) residues and by two bridging glutamate (Glu51 and Glu127) residues. This generates a highly symmetric centre that may be classified as a class II dinuclear iron centre and, as such, is closely related to the dinuclear iron centres of the R2 subunit of ribonucleotide reductase and the hydroxylase subunit of methane monooxygenase [56,57]. Recent structural studies of iron-free BFRs have shown that the residues at the ferroxidase centre are positioned to accept Fe^{2+} ions such that significant conformational changes do not occur upon binding iron. In the case of *Pseudomonas aeruginosa* bacterioferritin (BfrB) all residues except His130 were positioned ready to bind Fe^{2+} [58], while for *E. coli* BFR, all side chains of the ferroxidase centre residues were clearly in position to bind metal ions with no significant rearrangement [55]. Similar observations were made for the R2 subunit of ribonucleotide reductase [59] for which a complex hydrogen bonding network that stabilizes the metal-free form of the centre was proposed. Fe^{2+} binding to the apo-BFR ferroxidase centre leads to the release of four protons (two per metal ion), thus maintaining the charge balance of the centre [60]. Two of these protons presumably arise from the deprotonation of the histidine residues at the centre, while the origin of the remaining two is not clear, though it is likely that they are derived from two of the four glutamate residues at the centre (which would have unusually high pK_a values), suggesting that a hydrogen bonding network is likely to be important for the stabilization of the BFR centre in the absence of metal ions in an analogous fashion to the R2 subunit of ribonucleotide reductase. Binding of two divalent metal ions per apo-BFR subunit is believed to occur via a pore between helices A and C that connects the ferroxidase centre with the protein exterior, see Fig. 8. A recent structure of an engineered BFR subunit dimer (that
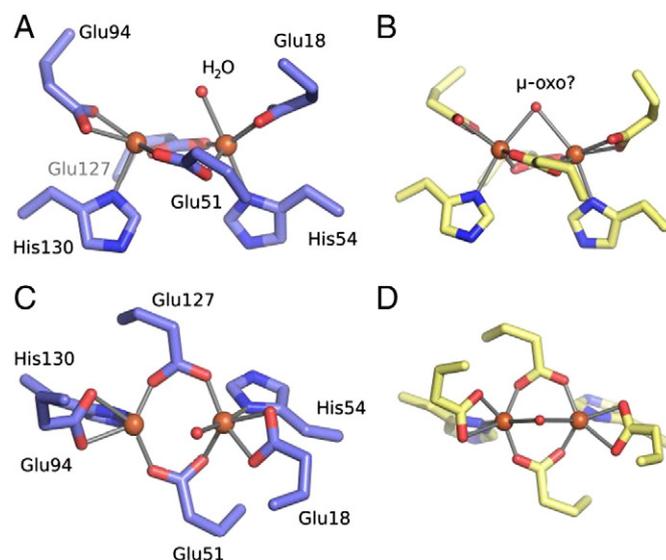

Fig. 4. Structure of Ftn proteins. Cartoon representations of A, the *E. coli* FtnA subunit dimer peptide backbone (pdb 1EUM), B, the overall structure of 24meric *E. coli* FtnA, and C, 24meric arrangement of *A. fulgidus* Ftn with a view down one of the super-pores (pdb 1SQ3).

Fig. 5. The heme site of BFR. Cartoon/sticks representation of the intra-dimer, inter-monomer heme binding site of *E. coli* BFR showing coordination via the two Met52 residues (one from each monomer).

Fig. 7. The ferroxidase centre of BFR. Sticks side on representations of A, the di-Fe^{2+}-form (pdb 3E1M) and B, bridged di-Fe^{3+}-form (pdb 3E1N) of the *E. coli* BFR ferroxidase centre. Overhead views of the di-Fe^{2+} and bridged di-Fe^{3+}-forms are shown in C and D, respectively.

cannot assemble further) revealed that a molecule of polyethylene glycol was bound in the pore [61].
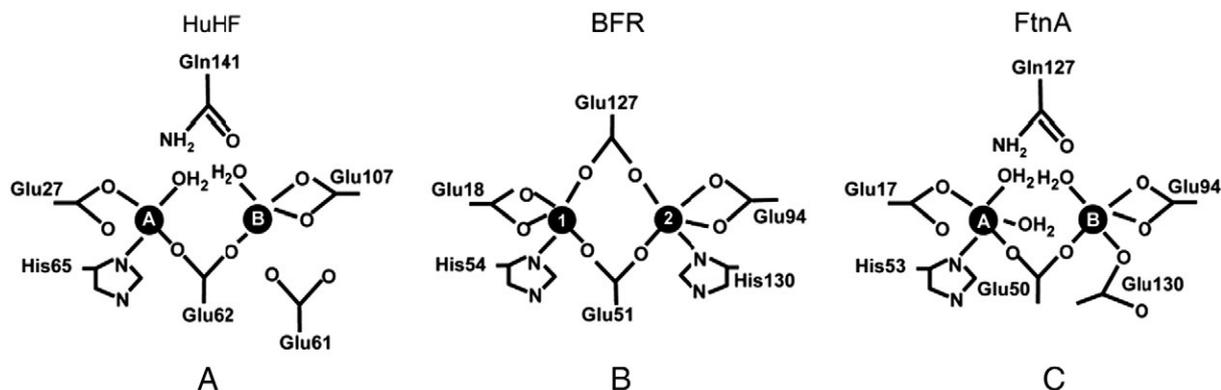
The ferroxidase centre of BFR has been structurally characterised in a number of iron-bound forms. Although the structure of BFR was first reported in 1994 [26], the first iron-bound structure was not described until 2003. In this study, the ferroxidase centre of as isolated *Desulfovibrio desulfuricans* BFR contained a bridged di-Fe^{3+} species with an inter-iron distance of 3.71 Å [28]. The identity of the bridging species could not be determined, and it was concluded that the structure likely represented a mixture of species containing terminal water ligands, a peroxo-intermediate and/or an oxo/hydroxo-bridge. Reduction of the centre with dithionite resulted in a di-Fe^{2+} centre with no bridging electron density and an inter-iron distance of 3.99 Å. Re-oxidation of the centre led to partial occupancy, see Section 4.1. Iron-bound forms of *Azotobacter vinelandii* BFR have also been reported. In one study, the centre was found with partial occupancy at the Fe1 site and full occupancy at the Fe2 site [29] (note that, here, the irons are referred to as 1 and 2, rather than A and B, so as to distinguish the class II diiron-type centre from the H-chain ferritin-type). In a second study, the two ferroxidase centre sites were equally (and essentially fully) occupied, with the two Fe^{3+} ions, ~3.5 Å apart and bridged by a water molecule [30]. This form was concluded to represent the oxidised state, with reduction by dithionite leading to a lengthening of the iron-iron distance to ~4 Å and the loss of His130 as a ligand to Fe2 together with a number of other concerted side chain rearrangements, including movement of Glu47. The BFR of *Rhodobacter*
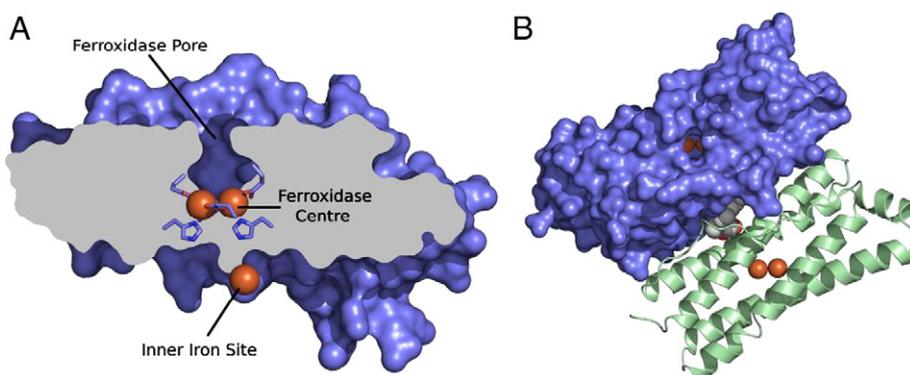
capsulatus has also been structurally characterised [27], and the ferroxidase centre was found to be only partially occupied (with an unknown metal), most likely due to the fact that the protein was exposed to the metal chelator EDTA during purification and crystal-lisation. In this structure, Glu18 (a ligand to the Fe1 site) was found to adopt two different orientations, possibly a consequence of the partial occupancy at this site.

The first high resolution structure of a BFR was that of the *E. coli* protein [26], in which the ferroxidase centre was occupied by two Mn^{2+} ions. Flexibility of coordination at the Fe2 site was observed such that, as in iron-bound *A. vinelandii* BFR, His130 was able to adopt a non-ligating conformation [62]. The structure of *E. coli* BFR containing a mixture of iron and zinc at the ferroxidase centre has also been solved. As well as revealing bidentate ligation of Glu18 at Fe1, the structure again indicated flexibility of amino acid residue side chains at Fe2, suggesting that this is a common feature of this site. Recently, di-Fe^{2+} and bridged di-Fe^{3+} structures of *E. coli* BFR were obtained from iron-soaking experiments using crystals of apo-BFR [55]. The di-Fe^{2+} structure was similar to other divalent metal ion forms of the protein (including the original Mn^{2+}-bound form), with an inter-iron distance of 3.71 Å, (Fig. 7A and C) a distance shorter than the 3.99 Å inter-iron distance in di-Fe^{2+} *D. desulfuricans* BFR [28]. Prolonged aerobic soaking resulted in a bridged di-Fe^{3+} ferroxidase centre, with an inter-iron distance of 3.63 Å [55], shorter than that reported for the di-Fe^{3+} form of the *D. desulfuricans* BFR

Fig. 6. The ferroxidase centres of ferritin family proteins. Schematic representations of the ferroxidase centres of A, Human H-chain ferritin, B, BFR (from *E. coli*) and, C, FtnA (from *E. coli*). The di-Fe^{2+} forms of the ferroxidase centres are depicted. For H-chain and FtnA centres, the models are based on structural information derived from di-Zn^{2+} forms of the centres [42,52], while for BFR, the model is derived directly from the di-Fe^{2+} structure [55].

Fig. 8. The ferroxidase centre pore of prokaryotic ferritins. A, A cross-section view of the *E. coli* BFR subunit viewed side on, showing the pore linking the ferroxidase centre with the outside of the protein. B, Space filled view from outside the protein down into the Fe^{2+}-containing ferroxidase centre of one BFR subunit. The other monomer of the subunit dimer is shown in cartoon format.

centre (3.71 Å). As for *D. desulfuricans* BFR, the origin of the additional 'bridging' electron density was not established unequivocally, but, importantly, the density was homogenous and consistent with a small molecule such as H_2O, OH^-, O_2, H_2O_2 or O^{2-}, rather than a mixture of species, and was therefore concluded to represent a μ-oxo or hydroxo bridged di-Fe^{3+} form of the ferroxidase centre (Fig. 7B and D), similar to those previously observed in the di-Fe^{3+} sites of other proteins such as ribonucleotide reductase, purple acid phosphatase, hemerythrin, and methane monooxygenase [56,57,63–65]. Such a conclusion is consistent with previous mechanistic studies of *E. coli* BFR, which indicated that a μ-oxo or hydroxo bridged di-Fe^{3+} form of the ferroxidase centre is generated (and is kinetically stable) following oxidation of Fe^{2+} ions at the centre [66,67].
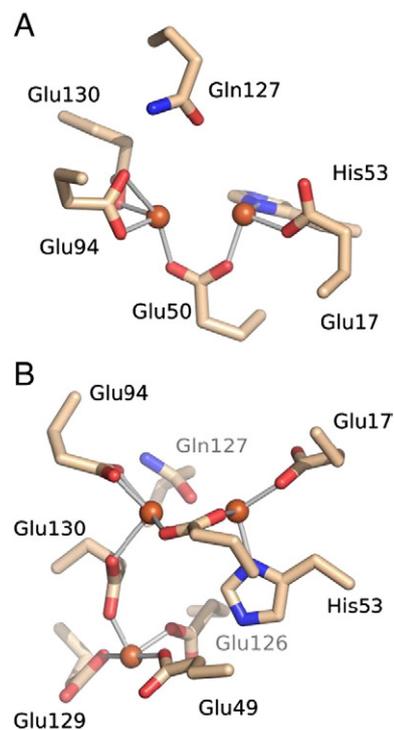
Although the Dps proteins (which are not discussed in detail here) typically have inter-subunit catalytic centres that are not related to those of ferritins, it is extremely interesting that the Dps-like proteins from the archaea *Sulfolobus solfataricus* and [68] *Pyrococcus furiosus* [69] and homologues all contain all of the residues that serve as ligands to the BFR ferroxidase centre. Indeed, the high resolution structure of the Dps-like protein from *Sulfolobus solfataricus* contained two metal ions at the centre (a mixture of zinc and iron) [70] and also revealed a pair of cysteine residues that could themselves cycle between thiol (reduced) and disulfide bonded (oxidised) forms. These observations raise important questions about the evolutionary relationships between Dps-like proteins and ferritins.

3.2.2. The Ftn ferroxidase centre

The ferroxidase centre of Ftn closely resembles that of H-chain ferritin and is, therefore, quite distinct from that of BFR. A high resolution structure of the iron-free form of the FtnA protein from *E. coli* has been solved, and, like BFR, the ferroxidase centre residues were found to be in a conformation similar to that found in metal-bound forms [42], suggesting that this may be a common feature of dinuclear iron centres. The structure of an iron bound form of the centre was also solved by soaking crystals of apo-FtnA in an Fe^{2+}-containing solution. Fe^{3+} bound at the FeA site was ligated by monodentate glutamate (Glu17) and histidine (His53) residues, and a bridging glutamate (Glu50). Fe^{3+} at site FeB was ligated by Glu50 and two monodentate glutamates (Glu94 and Glu130), see Figs. 1 and 9A. In addition, a water molecule was coordinated to FeA and a second water bridged the irons, which the authors suggested was likely to be an oxo- or hydroxo-bridge [42]. The inter-iron distance (3.24 Å), was significantly shorter than that observed at the BFR ferroxidase centre, and the occupancy of the FeB site was significantly lower than that of the FeA site. The coordination of FeB is different from that in H-chain: Glu130 is either an additional ligand or it replaces Glu61 (depending on whether Glu61 is actually a ligand to the FeB site of the H-chain centre (see above)). It should also be noted that Glu130 and Glu61 are derived from different parts of the sequences of H-chain and FtnA, respectively. Importantly, the dinuclear centre of FtnA is associated with an additional, closely located

iron site, FeC, discussed in detail in Section 3.3.2. Although the structure of a di-Fe^{2+} form of the FtnA centre is not yet available, soaking of apo-FtnA crystals in Zn^{2+} yielded a structure that likely resembles the di-Fe^{2+} form (shown schematically in Fig. 6C), with zero occupancy at the third iron site. The inter-metal distance was, as expected, lengthened to 3.43 Å [42].

Iron-bound forms of the Ftn homologue from *H. pylori*, rather confusingly referred to in some reports as Hpf, have been solved [44]. Iron was observed at the ferroxidase centre, but only the FeB site was significantly occupied. Surprisingly, soaking apo-crystals in Zn^{2+} or Ni^{2+}-containing solutions did not result in metal-binding at the centre, but Cd^{2+} ions were bound at both sites at full occupancy. The ferroxidase centre of the Ftn from the archaeon *Archaeoglobus fulgidis* was found to be partially occupied by what are believed to be Zn^{2+} ions following expression/overproduction in *E. coli* [12]. Iron soaking experiments led to an iron-bound form of the centre, with each iron bound by the equivalents of those at the *E. coli* FtnA centre, and an inter-iron distance of 3.18 Å, which is very close to those observed in the bridged di-Fe^{3+} form of the *E. coli* FtnA centre. The relatively low resolution of this structure prevented detailed determination of

Fig. 9. The ferroxidase centre and Site C of *E. coli* FtnA. Sticks representation of A, the bridged di-Fe^{3+}-form of the *E. coli* FtnA ferroxidase centre, and B, a rotated view from under the ferroxidase centre showing Fe^{3+} at the closely lying site C [42]. Note that water molecules are not shown. The pdb file was kindly provided by Prof. Peter Artymiuk (University of Sheffield).

solvent molecule/bridging ligands, although the electron density indicates that these are important features of the oxidised centre. As for *E. coli* FtnA, the third iron site, FeC, is also occupied (see Section 3.3.2). A second archeon Ftn from *P. furiosis* was recently structurally characterised [13]. The ferroxidase centre within crystals of as-isolated protein contained iron only at the FeA site. Iron at site FeB (and FeC) was only observed following soaking experiments, and even then, occupancy at site FeB was lower than that of FeA. The inter-iron distance was ~3.0 Å, shorter than in other Ftn structures but consistent with a di-Fe^{3+} centre. Soaking as isolated protein crystals in Zn^{2+} led to Zn^{2+} binding at the centre (and therefore at least partial displacement of iron).

3.3. Other protein-associated iron sites

3.3.1. The inner surface site of BFR

In addition to the ferroxidase centre, structural and mechanistic studies of BFR from *E. coli* identified an additional iron site on the inner face of the protein, associated with an aspartate (Asp50) and a histidine residue (His46), [55]. This internal iron site is 9.2 Å from the nearest ferroxidase centre iron, and 10.2 Å from the second, and clearly protrudes into the central cavity, Fig. 10. Maximum occupancy of the site was obtained following a Zn^{2+}/Fe^{2+} double soaking experiment with crystals of apo-BFR, resulting in Zn^{2+} ions at the ferroxidase centre and Fe^{2+} at the inner surface site, coordinated by only one oxygen from Asp50 and the ε-Nitrogen of His46, and up to three (partially) crystallographically ordered water molecules.

Studies of H46A, D50A single and H46A/D50A double variants revealed that the site is functionally significant. Each of the variants exhibited substantially reduced core mineralisation kinetics and reduced core capacities but were not affected in their ferroxidase centre reactivities [55]. Similar conclusions resulted from studies of an *E. coli* BFR variant in which subunit interactions are affected such that it cannot assemble beyond a subunit dimer [61]. Here, substitution of Asp50 and Asp126, another surface exposed residue (see Fig. 10), with glutamine resulted in only a small effect on the ferroxidase centre reaction, but a major decrease in the rate of mineralisation. These reports represent the first instances of site-directed variants of BFR in which core formation is inhibited but ferroxidase centre activity is not; *i.e.*, the mineralisation reaction (see Section 4.1) is selectively impaired in these variant proteins.

Alignment of BFR amino acid sequences showed that His46 and Asp50 are conserved to different extents. While an Asp or Glu residue is almost universally found at position 50, the His residue is not conserved. It is present in BFRs from γ-proteobacteria and cyanobacteria but is often substituted (in some cases by a non-ligating residue) in BFRs from other bacteria (Fig. 1). Thus, modified and/or alternative inner surface sites must exist in these BFRs. It is interesting to note that, although not present in all BFRs, the inner surface site of *E. coli* BFR is related to metal-binding sites previously observed in eukaryotic ferritins. A metal ion binding site on the inner surface of the K86Q variant of human H-chain ferritin (HuHF) was reported following a soak experiment in a solution containing Tb^{3+} [51]. The site involved coordination by Glu61 (the equivalent of Asp50 in BFR) and Glu64 (a lysine residue in BFR). Interestingly, His46 is also conserved in HuHF (His57), and a recent structural study of the apo form of a E27D/K86Q variant of HuHF following a Zn^{2+} soak revealed two metal sites on the inner surface, one of which was ligated by His57 and Glu61 [52]. Similar sites (again, amongst others) were also identified in mitochondrial ferritin (Mn^{2+} bound by His57 and Glu61) [54] and in mouse L-chain ferritin (Cd^{2+} bound by His53 and Glu57) as ligands [71]. The subunit structures of BFR and mitochondrial ferritin [54], the human H-chain [52], and the mouse L-chain [71] are superimposed in Fig. 11. For human H-chain and mitochondrial ferritins, the ligands almost overlay those of the BFR site, except for a Glu in place of Asp, perhaps indicating that these sites are also involved in Fe^{2+}-binding during core nucleation. The L-chain subunit lacks the dinuclear ferroxidase centre, and the His/Asp site is not conserved. However, a Cd^{2+} binding site with coordinating His and Glu
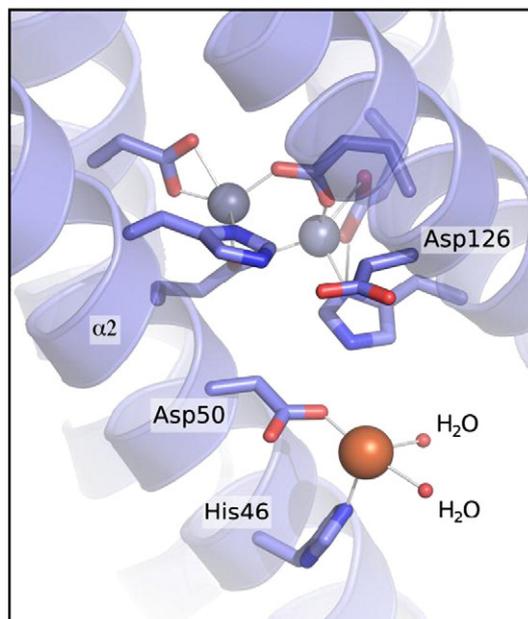

Fig. 10. The inner surface site of *E. coli* BFR. A sticks/cartoon representation of the inner surface iron site of *E. coli* BFR in which Fe^{2+} is coordinated by His46, Asp50 and crystallographically ordered water molecules (pdb 3E1M).
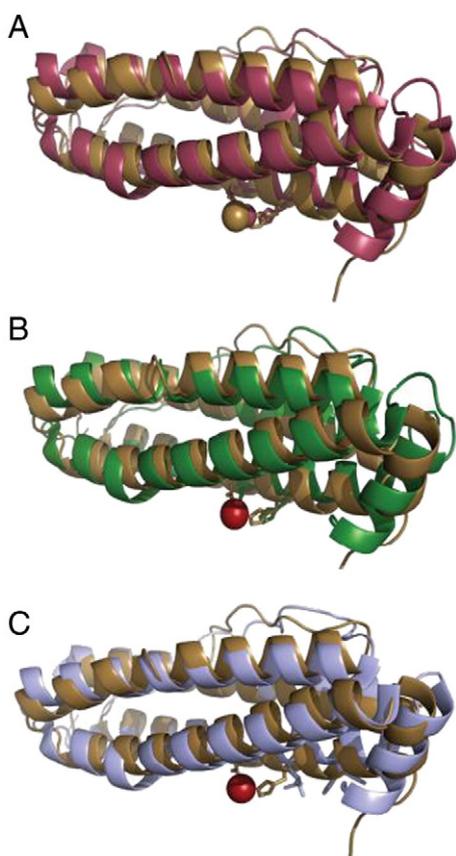
residues was identified in the structure of mouse L-chain, at a position shifted one turn of helix B towards the helix E end of the subunit. In each of these cases, an iron-bound form has not been reported, and the metal sites were identified as one of two or more sites at or close to the surface. Thus, the likely mechanistic significance of each site is less clear than in the case of *E. coli* BFR. However, the fact that this site occurs in both prokaryotic and eukaryotic ferritins points towards it having a functional role.

3.3.2. Site C of Ftn

An important difference between FtnA and H-chain ferritin was revealed in the iron-soaked structure of *E. coli* FtnA. In addition to the two ferroxidase centre iron sites, a third iron-binding site, site FeC (or site C) was observed [42]. Iron at this latter site is coordinated by Glu49, Glu126, Glu129 and Glu130 and two water molecules (Fig. 1). Notably, Glu130 is also a ligand to the FeB site and so bridges the FeB and FeC irons, see Fig. 9B. Also of interest is that Glu49 is equivalent to Asp50 in BFR (a ligand of the inner surface site iron) [42,72]. The FeB-FeC inter-iron distance is ~5.8 Å, though, as mentioned above, the occupancy of FeB is low relative to FeC.

Studies of site-directed variants of FtnA revealed that site C is not essential for rapid iron oxidation but that it does have an important effect on the characteristics of iron mineralisation [73]. Sequence comparisons revealed that the residues acting as ligands to FeC are highly conserved [13], indicating the functional importance of the site. Because the FeC site is not absolutely required for iron storage, it may play a more subtle role in iron movement into the protein cavity.

The structure of iron-soaked *H. pylori* Ftn (Hpf) did not contain iron at FeC although the amino acid ligands and their arrangement suggests that the site is present. The two archaea Ftn proteins with known structures also possess a site C that has been observed with iron-bound in the structure of each. In *A. fulgidis* Ftn, Fe^{3+} at site C is 5.96 Å away from FeB, with significant rearrangement of residues Glu51 and 131 (equivalent to Glu49 and 129 in *E. coli* FtnA) on going from the native crystals (in which the ferroxidase centre is believed to be Zn^{2+} bound) to the iron-bound form [12]. Although as isolated protein crystals of *P. furiosus* Ftn did not contain iron at site C, iron-soaked crystals did, with coordination by the same four Glu residues as in *E. coli* FtnA and a longer FeB to FeC distance (6.3 Å) [13]. As also observed in the structure of *E. coli* FtnA, site C was apparently occupied at the expense of site FeB.

Fig. 11. Structural comparison of the inner surface iron site of *E. coli* BFR with non-iron sites identified in vertebrate ferritins. Cartoon representation of a subunit of BFR showing the inner surface-bound Fe^{2+} ion (pdb 3E1M) coloured in sand yellow, with His46 and Asp50 shown in stick representation, superimposed on A, subunit of Zn^{2+}-soaked E27D K86Q human H-chain ferritin (pdb 2CIH), coloured in magenta His57 and Glu61 are shown in stick representation and the bound Zn^{2+} in magenta, and B, subunit of mitochondrial ferritin (pdb 1R03) coloured in green. His57 and Glu61 are shown in stick representation. The pdb file does not correspond to the Mn^{2+} soaked structure [54] and so the metal is not shown, C, subunit of mouse T125A L-chain ferritin (pdb 1LB3), coloured in blue. His53 and Glu57 are shown in sticks representation. The pdb file does not contain the Cd^{2+} ion reported [71] and so is not shown.

3.4. The iron mineral core

Ferritin proteins can accommodate polynuclear iron clusters within their central cavities. It is estimated that up to 4500 iron atoms could theoretically be stored as the mineral ferrihydrite [74], but as isolated proteins generally contain much less than this. Vertebrate ferritins, as isolated, generally contain 1000 - 3000 atoms of iron per molecule, while BFRs usually contain only 800 - 1500 iron atoms [5]. Furthermore, *in vitro* loading experiments have not been able to achieve iron clusters with more than ~3000 iron atoms; this result is attributable to low rates of mineralisation at high iron loadings which enables Fe^{2+} oxidation outside of the cavity to compete kinetically with intra-protein oxidation. Precise structural information for ferritin cores is lacking because preparations of iron-containing ferritins are generally poly-disperse with respect to their core component even though their protein components are homogeneous. This situation is probably a consequence of the high symmetry of the internal protein surface, which means that although the protein is aligned in the crystal, the iron mineral can be nucleated at potentially 24 different positions relative to it, leading to a smearing of electron density due to the mineral. This problem has thus far prevented determination of an X-ray structure of the mineral core within ferritins. The generally accepted structure for the crystalline iron core of ferritin is similar to that of the mineral ferrihydrite [75]. Precise structural information on ferrihydrite itself (i.e. not associated with ferritin) has proved difficult to obtain due to long range disorder, but

Michel and colleagues recently succeeded in obtaining a high resolution model of the mineral from pair distribution function analysis of total X-ray scattering [76]. From this analysis, these authors assigned the formula $Fe_{10}O_{14}(OH)_2$, and proposed a model involving a lattice in which 80% of the iron is octahedrally coordinated to oxygen and 20% is tetrahedrally coordinated, with the tetrahedral iron surrounded by octahedral iron. Although models of the ferritin core structure exist in which iron does occur with tetrahedral coordination [77], the majority of studies have suggested that only octahedral iron is present [75,78]; therefore, the true nature of the ferritin mineral remains unclear. Indeed, recent studies of horse spleen ferritin cores revealed a polyphasic structure (containing the minerals ferrihydrite, magnetite and hematite) and that the proportion of each varies with iron content, with ferrihydrite dominating as the core size increased [79].

The iron cores of prokaryotic ferritins exhibit considerable variability. BFR cores are generally referred to as 'iron-oxy-hydroxide-phosphate' and are, in general, far less well ordered than those of eukaryotic ferritins. Their mean core sizes are, however, similar [80] to those of eukaryotic ferritins, consistent with lower density essentially amorphous material. Studies of native *A. vinelandii* BFR have shown that there are fewer Fe-Fe contacts than occur with eukaryotic (horse) ferritin, and those that do occur are at a greater interatomic distance [81]. Furthermore, EXAFS data showed that each core Fe^{3+} ion of BFR had 5-6 phosphorus atoms at < 3.2 Å distance, consistent with Fe:P ratios of ~1.7:1 [81], thus supporting a model for the core in which phosphate is clearly an integral constituent. Native bacterial ferritin cores have not been investigated in detail, but studies of Ftn from *H. pylori* revealed that it contains significant amounts of iron and phosphate (Fe:P ratio of 1.4:1), leading to the conclusion that it has a BFR-like core structure [82]. Some phosphate is also typically found associated with eukaryotic ferritin cores but is largely associated with the surface of the mineral and does not appear to be an integral component [81]. *In vitro* experiments with BFR have shown that the properties of the core can be modulated between native and eukaryotic ferritin-like through the inclusion or omission of phosphate from the reconstitution reaction mixture [83,84], and reconstitution of *E. coli* FtnA also resulted in a ferrihydrite-like core [37]. Importantly, such experiments suggest that core morphology is controlled principally by the chemical composition of the medium in which mineralisation takes place.

The structural differences in core type in prokaryotic ferritins result in physical properties quite distinct from those of eukaryotic ferritins, particularly with regard to magnetic properties [85–90]. Even amongst BFR cores, there is variability with some exhibiting behaviour characteristic of superparamagnetism, a property usually associated with crystalline cores of eukaryotic ferritins [85,91], suggesting that pockets of more ordered material may be embedded, to a greater or lesser extent, within the amorphous mass.

4. Mechanisms of iron mineralisation

Understanding the processes by which the mineral iron core is laid down in ferritins has been a major research focus for the past 40 years. The majority of work has concerned eukaryotic ferritins, and a complex interplay of oxidation pathways has emerged. The catalytic activity of ferritins is associated with H-chain subunits and, in particular, the dinuclear ferroxidase centre [51,53,92,93]. At iron loading below or equal to that required to fill the ferroxidase centres, the key catalytic reaction occurs at the ferroxidase centre, leading to oxidation of the two Fe^{2+} ions and reduction of dioxygen to hydrogen peroxide (a two electron process) [93,94]. The oxidised form of the H-chain ferroxidase centre is not stable and undergoes a hydrolysis reaction leading to passage of the Fe^{3+} into the internal cavity and subsequent mineral formation. The ability of the ferroxidase centre to regenerate its apo-form and catalyse further Fe^{2+} oxidation [95–97] indicates that it acts as a 'gated iron pore' into the cavity, whereby iron transfer is coupled to oxidation of Fe^{2+} to Fe^{3+}. At high iron loadings, the principle site of catalysis switches from the

ferroxidase centre to the growing core surface [93,96,98] and results in the complete reduction of dioxygen to water (a four electron process). The observation of core-surface catalysed mineralisation led initially to the crystal growth model for core formation in which the core surface is the only catalytic site and the available core surface controls the kinetics of Fe^{2+} oxidation [99,100]. Addition of intermediate amounts of Fe^{2+} (*i.e.* 100-500 Fe^{2+} per molecule) results in consumption of some of the hydrogen peroxide produced at the ferroxidase centre in an Fe^{2+} oxidation reaction [93]. Thus, iron oxidation in eukaryotic H-chain ferritins occurs through a combination of these three pathways, depending on the amount of Fe^{2+} added.

For many years it was assumed that mineralisation in prokaryotic ferritins would take place via a similar H-chain-like mechanism. However, studies over the past twenty years have demonstrated that these proteins exhibit a diversity of mechanisms, some of which are very different to the H-chain model outlined above.
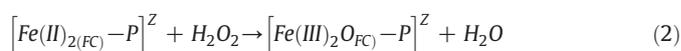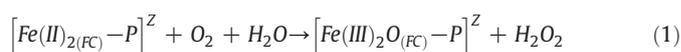
4.1. BFR

Despite the fact that BFRs have been isolated from a wide range of bacteria and high resolution structures are available for many, there is relatively little mechanistic information available for BFRs other than that from *E. coli*. In many cases, mechanistic information has been inferred from structural studies. Structural studies of *D. desulfuricans* BFR provided the first atomic detail of iron-bound forms of BFR (as the original structure of *E. coli* BFR contained Mn^{2+} ions [26]). As isolated, the ferroxidase centre was found to be present in a bridged di-Fe^{3+} form [28]. Upon reduction of crystals with excess dithionite, the centre was converted to a di-Fe^{2+} form, and subsequent exposure of crystals to dioxygen led to the observation of a centre containing iron at full occupancy only in the Fe2 position (coordinated by Glu56, Glu99, Glu132 and His135); iron at position Fe1 was depleted to 0 – 30% across all of the subunits. This finding led the authors to propose that iron had been transferred to the internal cavity, facilitated by a concerted movement of His59 and Glu132, which opened up a pore connecting the centre to the internal cavity. Such a gated iron pore mechanism would align BFR closely with the mechanism of eukaryotic H-chain ferritins. A similar mechanistic model was proposed on the basis of iron bound forms of *A. vinelandii* BFR. Liu and co-workers solved the structure of the protein containing partially occupied ferroxidase centres, with Fe1 significantly depleted relative to Fe2 [29]. In contrast, Swartz and co-workers crystallised the same protein in an as-isolated form but found that both sites of the ferroxidase centre were occupied and in an oxidised state (see Section 3.2) [30]. Reduction with dithionite led to an increase in the iron-iron distance and to changes in the Fe2 site coordination and beyond, such that His130 was no longer a ligand to the iron. Although re-oxidation of the centre did not lead to loss of iron (the oxidised form was re-generated), the redox-dependent conformational changes were interpreted as providing support for a mechanism in which the centre functions as a redox gated iron pore. The unusual observation of an iron atom bound at the four-fold channel also led these authors to suggest that Fe^{2+} enters the protein via the four fold channels, becomes oxidised at the ferroxidase centre before being incorporated into the growing mineral core.
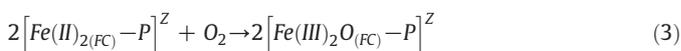
These mechanistic interpretations are based only on structural information, but it is important to combine such information with data from solution mechanistic studies of mineralisation. Recently, such a combined study of *P. aeruginosa* BfrB was reported [58], providing clear evidence in favour of the proposal that the BFR ferroxidase centre functions as a gated iron pore. However, a substantial body of mechanistic and structural data are available for *E. coli* BFR, and from this a different mechanistic picture emerges [55,66,67,101–103]. Mineralisation of *E. coli* BFR occurs via a mechanism consisting of three kinetically distinct phases. In the first (phase 1), two Fe^{2+} ions enter each of the 24 pre-organised but conformationally flexible unliganded ferroxidase centres. As first noted in the structure of *Desulfovibrio desulfuricans* BFR [28], each centre is located at the base of a pore that provides direct access to the centre from the

outside of the protein, see Fig. 8. Of particular interest is the fact that the pore is present in the structure of apo-BFR [55], strongly suggesting that this is the route for Fe^{2+}-binding at the centre.

Binding of Fe^{2+} to apo-BFR is followed, in the presence of dioxygen, by the oxidation of each di-Fe^{2+} centre (Fig. 7A and C) to generate a μ-oxo/hydroxo bridged di-Fe^{3+} form (Fig. 7B and D), with the concomitant reduction of dioxygen to hydrogen peroxide, phase 2 [67,102]. This reaction is a two electron reduction but the $Fe:O_2$ ratio of the ferroxidase centre reaction is 4:1, indicating that the reduction is a four electron process. This stoichiometry implies that two ferroxidase centres act together to reduce a single dioxygen to the oxidation state level of water, and that the subunit dimer may be the functional unit of the protein [67]. Hydrogen peroxide production was subsequently detected and was found to be a much better oxidant of Fe^{2+} at the ferroxidase centre than dioxygen [67,102]. Thus, reaction of dioxygen at one ferroxidase centre yields a bridged diferric centre and hydrogen peroxide, and the latter subsequently reacts at another ferroxidase centre to generate a second bridged diferric centre and water, see Eqs. (1) and (2).
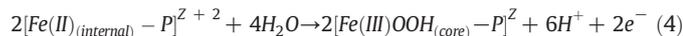
$$\left[Fe(II)_{2(FC)}-P\right]^Z + O_2 + H_2O \rightarrow \left[Fe(III)_2O_{(FC)}-P\right]^Z + H_2O_2 \qquad (1)$$

$$\left[Fe(II)_{2(FC)}-P\right]^Z + H_2O_2 \rightarrow \left[Fe(III)_2O_{FC}-P\right]^Z + H_2O \qquad (2)$$

where P indicates the BFR protein, FC indicates iron at the ferroxidase centre, and Z is the net charge on the protein. The net reaction of the two reactions in Eqs. (1) and (2) is given by Eq. (3):
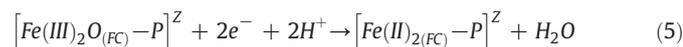
$$2\left[Fe(II)_{2(FC)}-P\right]^Z + O_2 \rightarrow 2\left[Fe(III)_2O_{(FC)}-P\right]^Z \qquad (3)$$

The resulting bridged di-Fe^{3+} centre is relatively stable, and a mechanism in which iron oxidised at the ferroxidase centre is subsequently transferred to the cavity can be ruled out [55,66,67,104]. The centre is modelled here as a μ-oxo-bridged rather than a hydroxo-bridged form, consistent with the pH independence of the ferroxidase oxidation reaction [67], but further studies are required to establish this. It is likely that the reaction in Eq. (1) proceeds via a diferric peroxo species, but the expected colour associated with this has not been detected in BFR so far. Thus, it is possible that such an intermediate is not formed, but perhaps more likely is that the species is too short-lived or its absorbance is too weak to detect. It is noteworthy that the inter-iron distance in the di-Fe^{2+} and the bridged di-Fe^{3+} forms of the ferroxidase centre are similar (3.71 and 3.63 Å, respectively). The catalytic cycling proposed here would be facilitated by a minimisation of structural reorganisation on changing oxidation states. Hence, the relatively small changes observed here upon oxidation may be functionally significant. Mechanistic and structural studies of *E. coli* BFR indicate that all 24 ferroxidase centres are functional during mineralisation. Fe^{2+}-binding/ oxidation at the centres is saturated at a level of 48 ions per protein, and in high resolution structures, fractional occupancies at the ferroxidase centres in both di-Fe^{2+} and bridged di-Fe^{3+} forms are close to 1. Therefore, the ferroxidase centre is the primary site of iron interaction with BFR and it is very likely that all ferroxidase centres are also active *in vivo*. Vertebrate ferritins exist as heteropolymers of H-chain (or H-chain-like) and L-chain subunits, the latter of which does not contain a catalytic ferroxidase centre. The relative proportions of each subunit type present in the 24mer have important consequences for the mineralisation properties of the ferritin, and there is significant variation in subunit compositions observed in different tissue types. Although some bacteria contain genes encoding more than one type of BFR, no evidence has yet been found that these assemble to form heteropolymers, and, in any case, virtually all contain a ferroxidase centre. So, functional fine-tuning through heteropolymer composition has not evolved in prokaryotes. Nevertheless, microbes may accomplish the same goal by another means, for example by expressing multiple BFR/ Ftn proteins in the same cell.

Phase 3 of mineralisation constitutes the actual formation of the iron core, and until recently it was quite unclear how a stable ferroxidase centre could drive formation of the core. Recent studies have provided significant new insight into this process. Fe^{2+} present in excess of that required to saturate the ferroxidase centre sites enters the central cavity *via* one or more of the channels in the protein coat which are located at the four-fold, three-fold and two-fold symmetry axes [26,28]. Which of these is most important for iron entry has not yet been established. Within the central cavity, Fe^{2+} ions bind on the inner face of the protein coat at internal nucleation sites. One such site, involving the side chains of Asp50 and His46, was recently identified by crystallographic studies of iron-soaked BFR crystals [55]. This inner surface site is located adjacent to the ferroxidase centre (Fig. 10).

A key question now is how does Fe^{2+} bound at this site, and perhaps other inner surface sites, become oxidised, leading to build up of an iron core? It has been demonstrated that the *E. coli* ferroxidase centre is required, and is therefore active, throughout core formation, and that the size of the existing mineral core is also important in determining the rate of iron oxidation [103]. To account for the importance of both the ferroxidase centre and the growing core surface it is proposed that Fe^{2+} bound at the internal surface site(s) becomes oxidised to Fe^{3+} and subsequently undergoes a hydrolysis reaction, Eq. (4):

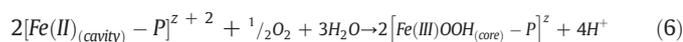$$2[Fe(II)_{(internal)} - P]^{Z+2} + 4H_2O \rightarrow 2[Fe(III)OOH_{(core)} - P]^Z + 6H^+ + 2e^- \quad (4)$$

where internal and core indicate iron at the inner surface site and within the core, respectively. The electrons resulting from Fe^{2+} oxidation in the cavity are channelled to the ferroxidase centre, where a di-Fe^{2+} centre is regenerated, Eq. (5):

$$\left[Fe(III)_2O_{(FC)} - P\right]^Z + 2e^- + 2H^+ \rightarrow \left[Fe(II)_{2(FC)} - P\right]^Z + H_2O \quad (5)$$

The resulting di-Fe^{2+} ferroxidase centre can now react again with dioxygen/hydrogen peroxide, and continues to operate in this catalytic cycle throughout core mineralisation. As the iron core builds up, it is reasonable to suppose that incoming Fe^{2+} will bind to the hydrated surface of the growing mineral, and that the mineral itself may act as a conducting wire to channel electrons resulting from the oxidation of the incoming Fe^{2+} to the ferroxidase centre. The ability of incoming Fe^{2+} to donate electrons into the core has been observed in Mössbauer studies of *A. vinelandii* BFR [105]. Alternatively, Fe^{2+} could continue to bind and become oxidised at inner surface sites that remain exposed and available (there are 24 such sites per BFR). Mutagenesis experiments indicate that Asp50 and His46 are important for mineralisation. Replacement of these residues with Ala resulted in unaltered activity of the ferroxidase centre, but a ~75–80% decrease in the rate of mineralisation [55]. These results suggest that this inner surface site is a key component of the electron transfer pathway connecting the core to the ferroxidase centre. However, the fact that mineralisation was not completely abolished in the absence of the inner surface site suggests that one or more alternative electron transfer pathways exist. Clearly, the characterisation of a *single* inner surface iron site also raises the question of how the ferroxidase centre obtains two electrons to become re-reduced. Several possible explanations can be proposed, including the existence of additional, as yet uncharacterised sites, and sequential oxidation of Fe^{2+} ions. The former possibility is supported by recent studies of a stable BFR subunit dimer in which Asp126 was found to play an important role in phase 3 mineralisation [61].

A key feature of the mechanism, which is summarized in Fig. 12A and B, is that, while the cavity is the site of Fe^{2+} oxidation, the ferroxidase centre is the site of dioxygen reduction. The overall core formation reaction is simply the sum of Eqs. (4) and (5), i.e. Eq. (6).

$$2[Fe(II)_{(cavity)} - P]^{z+2} + {}^1\!/_2O_2 + 3H_2O \rightarrow 2\left[Fe(III)OOH_{(core)} - P\right]^z + 4H^+ \quad (6)$$
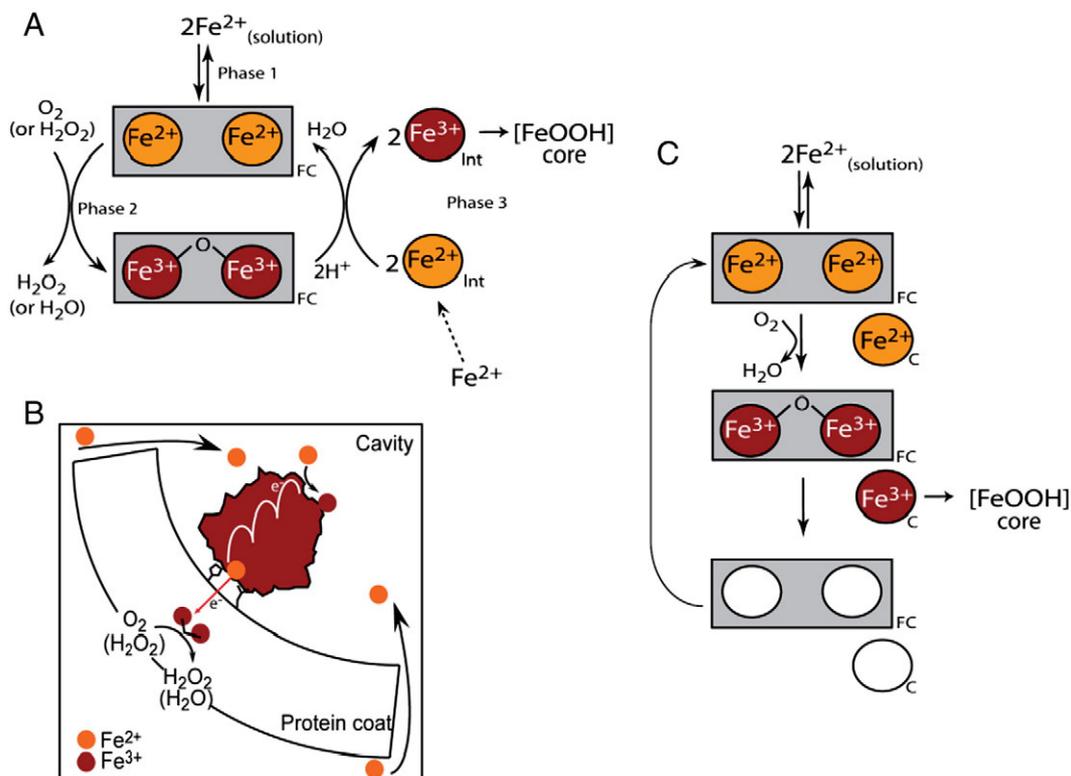
Phosphate is an integral component of the BFR core (see Section 3.4), but most *in vitro* studies of BFRs have been carried out in the absence of phosphate, leading to the formation of ferritin-like mineral cores. Studies of the effect of phosphate on mineralisation showed that it significantly increased the rate of phase 3 core formation [84], but not of phase 2. Consistent with this, phosphate was also shown to be important for promoting electron transfer reactions at the core surface [105].

In summary, studies of *E. coli* BFR over the past 20 years have led to an advanced understanding of the mechanism of mineralisation. The central focus of this mechanism is the cycling of the ferroxidase centre between the di-Fe^{2+} and μ-oxo/hydroxo bridged di-Fe^{3+} forms as the site is first oxidised by dioxygen/hydrogen peroxide and subsequently reduced by electrons transferred from Fe^{2+} ions located within the central cavity. The recently described functionally important inner surface site may play a dual role as the initiation point for core nucleation and as a facilitator for redox communication between the ferroxidase centre and the growing iron mineral core.

4.2. Ftn

E. coli FtnA is, in mechanistic terms, the best characterised of the bacterial ferritins [40–43,73,106]. Core mineralisation is proposed to occur via a mechanism similar to that of eukaryotic H-chain ferritin but which is complicated by the presence of site C [42]. Fe^{2+} binding at the ferroxidase centre in the presence of dioxygen leads to iron oxidation. This reaction proceeds via a coloured intermediate with absorption maxima at 370 and 600 nm [73,107]. This is not due to the direct binding of nearby tyrosine (Tyr24) to iron at the centre, as substitution of the tyrosine did not affect the appearance of the intermediate. The intermediate is likely to be a diferric peroxo species, as judged by the similarity of the Ftn reaction with that of human H-chain ferritin [108]. The intermediate decays to generate a μ-oxo-bridged Fe^{3+} dimer, which is proposed to convert further to a μ-hydroxo-bridged dimer [41,106]. Somewhat puzzlingly, the initial oxidation reaction has an iron:dioxygen ratio of 3–4, compared to 2 for eukaryotic H-chain ferritins [73]. This observation probably results from the presence of site C, and it is proposed that there may be a fourth, uncharacterised site for Fe^{2+} oxidation that would lead to reduction of dioxygen to water rather than hydrogen peroxide. Consistent with this is the observation that the iron:dioxygen stoichiometry dropped to 2 when site C residues were substituted. Once oxidised, iron at the ferroxidase centre is proposed to migrate into the central cavity where core mineralisation occurs. However, the flux of iron through the ferroxidase centre of FtnA (i.e. the regeneration of the centre) appears to be much slower than for eukaryotic H-chain, as judged from the fact that additions of Fe^{2+} beyond that required to saturate the ferroxidase centres are oxidised at a significantly diminished rate relative to the initial addition of iron to the apo-protein; such a difference is not observed for H-chain ferritins [73]. Importantly, an FtnA variant lacking site C exhibited only a small decrease in oxidation rate, indicating that site C is not essential. However, it appears that site C is important in controlling iron flux through the ferroxidase centre, because loss of site C resulted in a more rapid regeneration of the centre. The authors proposed that the lower rate of Fe^{2+} oxidation and core mineralisation that result from the presence of site C confers the advantage that iron remains at the ligand-accessible ferroxidase centre longer and that this could be important for satisfying cellular iron requirements. A further advantage is that hydrogen peroxide is not generated [73]. Structural and biochemical studies of *H. pylori* Ftn led to the proposal that mineralisation at low levels of iron is dominated by the ferroxidase centre reaction, while at higher iron loadings the mineral surface dominates [44]. Furthermore, based on the observation of an iron ion bound in the four-fold channel by four symmetry-related His149 residues, the authors suggest that these channels are the route for iron into the central cavity. The mineralisation mechanism for bacterial Ftn proteins is summarised in Fig. 12C.

Recent studies of the archaeon Ftn from *P. furiosus* have provided significant new insight into the mechanism of mineralisation in Ftn

Fig. 12. Mechanisms of mineralisation in prokaryotic ferritins. A and B, Schematic representation of mineralisation in *E. coli* BFR. The model shows in A the mechanism of core nucleation broken down into three distinct steps or phases. In phase 1, Fe^{2+} ions bind at the ferroxidase centre (labelled FC) and become oxidised in phase 2. In phase 3, Fe^{2+} bound at the internal, inner surface site (labelled Int) is oxidised, with electrons channelled to the ferroxidase centre, which is re-reduced. This mechanism continues to operate throughout core formation as illustrated in B, where incoming Fe^{2+} ions are oxidised at the core surface and the resulting electrons are channelled to the ferroxidase centre via a pathway that involves the inner surface iron site. Thus, the ferroxidase centre operates as a true catalytic centre. Note that this mechanism does not require that the core particle(s) remain permanently bound to the protein surface. A similar mechanism appears to operate in *P. furiosus* Ftn (see main text for details). C, Schematic representation of mineralisation in *E. coli* FtnA. Fe^{2+} ions bind at the ferroxidase centre and site C (labelled C) and become oxidised, in the presence of oxygen, generating an unstable di-Fe^{3+} form at the ferroxidase centre. Fe^{3+} ions at site C and the ferroxidase centre are transferred to the internal cavity where they nucleate, or become incorporated into, the mineral iron core. The apo-form of the ferroxidase centre/site C is now ready to accept further Fe^{2+} ions. Thus, the ferroxidase centre acts as a gated iron pore.

proteins. Kinetic experiments showed that the oxidation of the initial 48 Fe^{2+} per protein were distinct, in terms of rate, from subsequent additions. Studies of pre-loaded Ftn samples showed that rates of oxidation did not recover to those of the protein containing no iron (apo-protein), consistent with a very slow or negligible regeneration of the ferroxidase centre to its apo-form [109]. Stability of the oxidised ferroxidase centre was further demonstrated through redox titration experiments followed by electron paramagnetic resonance spectroscopy, which revealed that a mixed valence Fe^{3+}–Fe^{2+} centre could be readily generated, and that occupancy of the centre was not redox sensitive [110]. Dioxygen consumption experiments showed that the ferroxidase centre reaction proceeds with an iron:dioxygen ratio of ~2, indicating that hydrogen peroxide is generated during the ferroxidase centre reaction. This ratio remained constant for subsequent additions of 48 Fe^{2+} ions per protein and increased to ~3 for additions of 300 Fe^{2+} ions, from which it was concluded that hydrogen peroxide generated during oxidation was able to oxidise some of the Fe^{2+}. These results are inconsistent with a mechanism in which the ferroxidase centre functions as a gated iron pore, as shown for *E. coli* FtnA. Furthermore, it was concluded that the growing mineral core does not catalyse Fe^{2+} oxidation independently of the ferroxidase centre. These results led the authors to propose that the ferroxidase centre functions as a stable catalytic site, becoming re-reduced by electrons derived from the oxidation of Fe^{2+} to Fe^{3+} at nearby sites (e.g. site C) with resulting Fe^{3+} forming the iron core. Although the authors suggest that the *P. furiosus* Ftn mechanism represents a novel type of mineralisation mechanism, there is currently little to distinguish it, apart from the structural details, from that of the BFR mechanism described above. However, it is indeed

remarkable that, in terms of mechanism, *P. furiosus* Ftn is much more similar to *E. coli* BFR than to *E. coli* FtnA, see Fig. 12.

5. Concluding remarks and future challenges

From the substantial literature describing mechanistic studies of different ferritins, it is clear that a catalytic centre for Fe^{2+} oxidation, routes for Fe^{2+} access into the central cavity, and the ability to efficiently nucleate the iron core are common requirements for all ferritins. However, the specific structural and mechanistic details vary significantly between different ferritins. The ferroxidase centre of BFRs and Ftns are quite distinct from each other and from those of eukaryotic H-chain ferritins. Likewise, iron sites close to, or on the inside of, the protein coat are also variable: sites in BFR and Ftn proteins, which are the only ferritins for which functionally important iron sites outside of the ferroxidase centre have been structurally characterised, are distinct. While the Ftn site C is well conserved amongst Ftn proteins, the inner surface site identified in *E. coli* BFR is not present in all BFRs, and so alternative sites must exist amongst other BFRs. Even in BFRs with similar structures, significant mechanistic differences are apparent: structural and solution studies of the BFRs from *E. coli* and *P. aeruginosa* clearly show that these proteins are mechanistically distinct. Likewise, the Ftn proteins characterised so far exhibit very similar structures (with the exception of the unusual 2,3 symmetry of *A. fulgidis* Ftn) and all contain a very similar ferroxidase centre and associated site C, but the two Ftn proteins that have been best characterised mechanistically appear to be very different, suggesting that other differences must be important for determining the mineralisation mechanism. A major future challenge will be to gather

mechanistic and structural information on a wider range of BFRs and Ftns to determine the extent of structural and mechanistic variations, and the factors important in controlling them.

Acknowledgements

References

[1] P. Aisen, C. Enns, M. Wessling-Resnick, Chemistry and biology of eukaryotic iron metabolism, Int. J. Biochem. Cell Biol. 33 (2001) 940–959.
[2] M.A. Kohanski, D.J. Dwyer, B. Hayete, C.A. Lawrence, J.J. Collins, A common mechanism of cellular death induced by bactericidal antibiotics, Cell 130 (2007) 797–810.
[3] S.C. Andrews, A.K. Robinson, F. Rodriguez-Quinones, Bacterial iron homeostasis, FEMS Microbiol. Rev. 27 (2003) 215–237.
[4] N.D. Chasteen, Ferritin. Uptake, storage, and release of iron, Met. Ions Biol. Syst. Vol 35 (1998) 479–514.
[5] A. Lewin, G.R. Moore, N.E. Le Brun, Formation of protein-coated iron minerals, Dalton Trans. (2005) 3597–3610.
[6] E.C. Theil, M. Matzapetakis, X.F. Liu, Ferritins: iron/oxygen biominerals in protein nanocages, J. Biol. Inorg. Chem. 11 (2006) 803–810.
[7] P.M. Harrison, P. Arosio, Ferritins: molecular properties, iron storage function and cellular regulation, Biochim. Biophys. Acta-Bioenerg. 1275 (1996) 161–203.
[8] E.C. Theil, The ferritin family of iron storage proteins, Adv. Enzymol. Relat. Areas Mol. Biol. 63 (1990) 421–449.
[9] R.A. Grant, D.J. Filman, S.E. Finkel, R. Kolter, J.M. Hogle, The crystal structure of Dps, a ferritin homolog that binds and protects DNA, Nat. Struct. Biol. 5 (1998) 294–303.
[10] A. Ilari, S. Stefanini, E. Chiancone, D. Tsernoglou, The dodecameric ferritin from Listeria innocua contains a novel intersubunit iron-binding site, Nat. Struct. Biol. 7 (2000) 38–43.
[11] E. Chiancone, P. Ceci, The multifaceted actions of Dps proteins to combat bacterial stress conditions: detoxification of iron and hydrogen peroxide and DNA binding Biochim. Biophys. Acta this issue. doi:10.1016/j.bbagen.2010.01.013.
[12] E. Johnson, D. Cascio, M.R. Sawaya, M. Gingery, I. Schroder, Crystal structures of a tetrahedral open pore ferritin from the hyperthermophilic Archaeon Archaeoglobus fulgidus, Struct. Fold. Des. 13 (2005) 637–648.
[13] J. Tatur, W.R. Hagen, P.M. Matias, Crystal structure of the ferritin from the hyperthermophilic archaeal anaerobe Pyrococcus furiosus, J. Biol. Inorg. Chem. 12 (2007) 615–630.
[14] S.C. Andrews, The ferritin superfamily: structure, function and evolution of the biological iron storeman, Biochim. Biophys. Acta submitted for publication.
[15] H. Abdul-Tehrani, A.J. Hudson, Y.S. Chang, A.R. Timms, C. Hawkins, J.M. Williams, P.M. Harrison, J.R. Guest, S.C. Andrews, Ferritin mutants of Escherichia coli are iron deficient and growth impaired, and fur mutants are iron deficient, J. Bacteriol. 181 (1999) 1415–1428.
[16] J. Velayudhan, M. Castor, A. Richardson, K.L. Main-Hester, F.C. Fang, The role of ferritins in the physiology of Salmonella enterica sv. Typhimurium: a unique role for ferritin B in iron-sulphur cluster repair and virulence, Mol. Microbiol. 63 (2007) 1495–1507.
[17] D. Expert, A. Boughammoura, T. Franza, Siderophore-controlled iron assimilation in the enterobacterium Erwinia chrysanthemi evidence for the involvement of bacterioferritin and the Suf iron–sulfur cluster assembly machinery, J. Biol. Chem. 283 (2008) 36564–36572.
[18] B. Waidner, S. Greiner, S. Odenbreit, H. Kavermann, J. Velayudhan, F. Stahler, J. Guhl, E. Bisse, A.H.M. van Vliet, S.C. Andrews, J.G. Kusters, D.J. Kelly, R. Haas, M. Kist, S. Bereswill, Essential role of ferritin Pfr in Helicobacter pylori iron metabolism and gastric colonization, Infect. Immun. 70 (2002) 3923–3929.
[19] S.N. Wai, K. Nakayama, K. Umene, T. Moriya, K. Amako, Construction of a ferritin-deficient mutant of Campylobacter jejuni: contribution of ferritin to iron storage and protection against oxidative stress, Mol. Microbiol. 20 (1996) 1127–1134.
[20] R.R. Edson, C.J. Smith, Transcriptional regulation of the Bacteroides fragilis ferritin gene (ftnA) by redox stress, Microbiology 150 (2004) 2125–2134.
[21] S. Shcolnick, T.C. Summerfield, L. Reytman, L.A. Sherman, N. Keren, The mechanism of iron homeostasis in the unicellular cyanobacterium Synechocystis sp PCC 6803 and its relationship to oxidative stress, Plant Physiol. 150 (2009) 2045–2056.
[22] C.Y. Chen, S.A. Morse, Neisseria gonorrhoeae bacterioferritin: structural heterogeneity, involvement in iron storage and protection against oxidative stress, Microbiology 145 (1999) 2967–2975.
[23] E.I. Stiefel, G.D. Watt, Azotobacter cytochrome-b₅₅₇.₅ is a bacterioferritin, Nature 279 (1979) 81–83.
[24] S.C. Andrews, Iron storage in bacteria, Adv. Microb. Physiol. 40 (1998) 281–351.
[25] C.V. Romao, P.N. da Costa, S. Macedo, E. Mitchell, P.M. Matias, E. Melo, M.Y. Liu, A.V. Xavier, P. Lindley, J. LeGall, M.A. Carrondo, L.M. Saraiva, M. Teixeira, A bacterioferritin from the sulphate reducing bacterium Desulfovibrio desulfuricans ATCC 27774, with a novel haem cofactor, J. Inorg. Biochem. 86 (2001) 405–405.

[26] F. Frolow, A.J. Kalb, J. Yariv, Structure of a unique twofold symmetrical heme-binding site, Nat. Struct. Biol. 1 (1994) 453–460.
[27] D. Cobessi, L.S. Huang, M. Ban, N.G. Pon, F. Daldal, E.A. Berry, The 2.6 angstrom resolution structure of Rhodobacter capsulatus bacterioferritin with metal-free dinuclear site and heme iron in a crystallographic 'special position', Acta Crystallogr. D Biol. Crystallogr. 58 (2002) 29–38.
[28] S. Macedo, C.V. Romao, E. Mitchell, P.M. Matias, M.Y. Liu, A.V. Xavier, J. LeGall, M. Teixeira, P. Lindley, M.A. Carrondo, The nature of the di-iron site in the bacterioferritin from Desulfovibrio desulfuricans, Nat. Struct. Biol. 10 (2003) 285–290.
[29] H.L. Liu, H.N. Zhou, W.M. Xing, J.F. Zhao, S.X. Li, J.F. Huang, R.C. Bi, 2.6 angstrom resolution crystal structure of the bacterioferritin from Azotobacter vinelandii, FEBS Lett. 573 (2004) 93–98.
[30] L. Swartz, M. Kuchinskas, H.Y. Li, T.L. Poulos, W.N. Lanzilotta, Redox-dependent structural changes in the Azotobacter vinelandii bacterioferritin: new insights into the ferroxidase and iron transport mechanism, Biochemistry 45 (2006) 4421–4428.
[31] A. van Eerde, S. Wolternik-van Loo, J. van der Oost, B.W. Dijkstra, Fortuitous structure determination of 'as-isolated' Escherichia coli bacterioferritin in a novel crystal form, Acta Crystallogr. Sect. F Struct. Biol. Cryst.Commun. 62 (2006) 1061–1066.
[32] V. Gupta, R.K. Gupta, G. Khare, D.M. Salunke, A.K. Tyagi, Crystal structure of BfrA from Mycobacterium tuberculosis: incorporation of selenomethionine results in cleavage and demetallation of haem, Plos One 4 (2009).
[33] G.R. Moore, F.H.A. Kadir, F.K. Almassad, N.E. Le Brun, A.J. Thomson, C. Greenwood, J.N. Keen, J.B.C. Findlay, Structural heterogeneity of Pseudomonas aeruginosa bacterioferritin, Biochem. J. 304 (1994) 493–497.
[34] C.D. Miller, Y.C. Kim, M.K. Walsh, A.J. Anderson, Characterization and expression of the Pseudomonas putida bacterioferritin alpha subunit gene, Gene 247 (2000) 199–207.
[35] N. Keren, R. Aurora, H.B. Pakrasi, Critical roles of bacterioferritins in iron storage and proliferation of cyanobacteria, Plant Physiol. 135 (2004) 1666–1673.
[36] M.A. Carrondo, Ferritins, iron uptake and storage from the bacterioferritin viewpoint, EMBO J. 22 (2003) 1959–1968.
[37] A.J. Hudson, S.C. Andrews, C. Hawkins, J.M. Williams, M. Izuhara, F.C. Meldrum, S. Mann, P.M. Harrison, J.R. Guest, Overproduction, purification and characterization of the Escherichia coli ferritin, Eur. J. Biochem. 218 (1993) 985–995.
[38] S. Clerte, A. Dautant, B.L. d'Estaintot, B. Gallois, Y. Mizunoe, S.N. Wai, G. Precigoux, Expression, purification, crystallization and preliminary X-ray diffraction results from Campylobacter jejuni ferritin, Acta Crystallogr. D Biol. Crystallogr. 55 (1999) 299–301.
[39] D.B. Ratnayake, S.N. Wai, Y.X. Shi, K. Amako, H. Nakayama, K. Nakayama, Ferritin from the obligate anaerobe Porphyromonas gingivalis: purification, gene cloning and mutant studies, Microbiology 146 (2000) 1119–1127.
[40] A. Treffry, Z.W. Zhao, M.A. Quail, J.R. Guest, P.M. Harrison, The use of zinc(II) to probe iron binding and oxidation by the ferritin (EcFtnA) of Escherichia coli, J. Biol. Inorg. Chem. 3 (1998) 682–688.
[41] E.R. Bauminger, A. Treffry, M.A. Quail, Z.W. Zhao, I. Nowik, P.M. Harrison, Stages in iron storage in the ferritin of Escherichia coli (EcFtnA): analysis of Mössbauer spectra reveals a new intermediate, Biochemistry 38 (1999) 7791–7802.
[42] T.J. Stillman, P.D. Hempstead, P.J. Artymiuk, S.C. Andrews, A.J. Hudson, A. Treffry, J.R. Guest, P.M. Harrison, The high-resolution X-ray crystallographic structure of the ferritin (EcFtnA) of Escherichia coli; comparison with human H ferritin (HuHF) and the structures of the Fe³⁺ and Zn²⁺ derivatives, J. Mol. Biol. 307 (2001) 587–603.
[43] F. Bou-Abdallah, M.R. Woodhall, A. Velazquez-Campoy, S.C. Andrews, N.D. Chasteen, Thermodynamic analysis of ferrous ion binding to Escherichia coli ferritin EcFtnA, Biochemistry 44 (2005) 13837–13846.
[44] K.J. Cho, H.J. Shin, J.H. Lee, K.J. Kim, S.S. Park, Y. Lee, C. Lee, K.H. Kim, The crystal structure of ferritin from Helicobacter pylori reveals unusual conformational changes for iron uptake, J. Mol. Biol. 390 (2009) 83–98.
[45] M.R. Cheesman, A.J. Thomson, C. Greenwood, G.R. Moore, F. Kadir, Bis-methionine axial ligation of heme in bacterioferritin from Pseudomonas aeruginosa, Nature 346 (1990) 771–773.
[46] G.N. George, T. Richards, R.E. Bare, Y.J. Gea, R.C. Prince, E.I. Stiefel, G.D. Watt, Direct observation of bis-sulfur ligation to the heme of bacterioferritin, J. Am. Chem. Soc. 115 (1993) 7716–7718.
[47] R. Aranda, C.E. Worley, M. Liu, E. Bitto, M.S. Cates, J.S. Olson, B. Lei, G.N. Phillips, Bis-methionyl coordination in the crystal structure of the heme-binding domain of the streptococcal cell surface protein Shp, J. Mol. Biol. 374 (2007) 374–383.
[48] S.C. Andrews, N.E. Le Brun, V. Barynin, A.J. Thomson, G.R. Moore, J.R. Guest, P.M. Harrison, Site-directed replacement of the coaxial heme ligands of bacterioferritin generates heme-free variants, J. Biol. Chem. 270 (1995) 23268–23274.
[49] S.K. Weeratunga, C.E. Gee, S. Lovell, Y.H. Zeng, C.L. Woodin, M. Rivera, Binding of Pseudomonas aeruginosa apobacterioferritin-associated ferredoxin to bacterioferritin B promotes heme mediation of electron delivery and mobilization of core mineral iron, Biochemistry 48 (2009) 7420–7431.
[50] S.H. Banyard, D.K. Stammers, P.M. Harrison, Electron-density map of apoferritin at 2.8 Å resolution, Nature 271 (1978) 282–284.
[51] D.M. Lawson, P.J. Artymiuk, S.J. Yewdall, J.M.A. Smith, J.C. Livingstone, A. Treffry, A. Luzzago, S. Levi, P. Arosio, G. Cesareni, C.D. Thomas, W.V. Shaw, P.M. Harrison, Solving the structure of human H-ferritin by genetically engineering intermolecular crystal contacts, Nature 349 (1991) 541–544.
[52] L. Toussaint, L. Bertrand, L. Hue, R.R. Crichton, J.P. Declercq, High-resolution X-ray structures of human apoferritin H-chain mutants correlated with their activity and metal-binding sites, J. Mol. Biol. 365 (2007) 440–452.
[53] D.M. Lawson, A. Treffry, P.J. Artymiuk, P.M. Harrison, S.J. Yewdall, A. Luzzago, G. Cesareni, S. Levi, P. Arosio, Identification of the ferroxidase center in ferritin, FEBS Lett. 254 (1989) 207–210.

[54] B.L. d'Estaintot, S. Paolo, T. Granier, B. Gallois, J.M. Chevalier, G. Precigoux, S. Levi, P. Arosio, Crystal structure and biochemical properties of the human mitochondrial ferritin and its mutant Ser144Ala, J. Mol. Biol. 340 (2004) 277–293.

[55] A. Crow, T.L. Lawson, A. Lewin, G.R. Moore, N.E. Le Brun, Structural basis for iron mineralisation by bacterioferritin, J. Am. Chem. Soc. 131 (2009) 6808–6813.

[56] P. Nordlund, B.M. Sjoberg, H. Eklund, 3-Dimensional structure of the free-radical protein of ribonucleotide reductase, Nature 345 (1990) 593–598.

[57] A.C. Rosenzweig, C.A. Frederick, S.J. Lippard, P. Nordlund, Crystal structure of a bacterial nonheme iron hydroxylase that catalyzes the biological oxidation of methane, Nature 366 (1993) 537–543.

[58] S.K. Weeratunga, S. Lovell, H. Yao, K.P. Battaile, C.J. Fischer, C.E. Gee, M. Rivera, Structural studies of bacterioferritin B from Pseudomonas aeruginosa suggest a gating mechanism for iron uptake via the ferroxidase center, Biochemistry (2010), doi:10.1021/bi9015204.

[59] A. Aberg, P. Nordlund, H. Eklund, Unusual clustering of carboxyl side chains in the core of iron-free ribonucleotide reductase, Nature 361 (1993) 276–278.

[60] N.E. Le Brun, A.M. Keech, M.R. Mauk, A.G. Mauk, S.C. Andrews, A.J. Thomson, G.R. Moore, Charge compensated binding of divalent metals to bacterioferritin: H+ release associated with cobalt(II) and zinc(II) binding at dinuclear metal sites, FEBS Lett. 397 (1996) 159–163.

[61] S.G. Wong, S.A.L. Tom-Yew, A. Lewin, N.E. Le Brun, G.R. Moore, M.E.P. Murphy, A. G. Mauk, Structural and mechanistic studies of a stabilized subunit dimer variant of Escherichia coli bacterioferritin identify residues required for core formation, J. Biol. Chem. 284 (2009) 18873–18881.

[62] F. Frolow, A.J. Kalb, Cytochrome b_1-bacterioferritins, in: A. Messerschmidt (Ed.), Handbook of Metalloproteins Wiley, New York, 2001, pp. 782–790.

[63] Y. Lindqvist, E. Johansson, H. Kaija, P. Vihko, G. Schneider, Three-dimensional structure of a mammalian purple acid phosphatase at 2.2 Å resolution with a mu-(hydr)oxo bridged di-iron center, J. Mol. Biol. 291 (1999) 135–147.

[64] N. Strater, T. Klabunde, P. Tucker, H. Witzel, B. Krebs, Crystal structure of a purple acid phosphatase containing a dinuclear Fe(III)–Zn(II) active site, Science 268 (1995) 1489–1492.

[65] M.A. Holmes, I. Letrong, S. Turley, L.C. Sieker, R.E. Stenkamp, Structures of deoxy and oxy hemerythrin at 2.0 Å resolution, J. Mol. Biol. 218 (1991) 583–593.

[66] N.E. Le Brun, M.T. Wilson, S.C. Andrews, J.R. Guest, P.M. Harrison, A.J. Thomson, G. R. Moore, Kinetic and structural characterization of an intermediate in the biomineralization of Bacterioferritin, FEBS Lett. 333 (1993) 197–202.

[67] X. Yang, N.E. Le Brun, A.J. Thomson, C.R. Moore, N.D. Chasteen, The iron oxidation and hydrolysis chemistry of Escherichia coli bacterioferritin, Biochemistry 39 (2000) 4915–4923.

[68] B. Wiedenheft, J. Mosolf, D. Willits, M. Yeager, K.A. Dryden, M. Young, T. Douglas, An archaeal antioxidant: characterization of a Dps-like protein from Sulfolobus solfataricus, Proc. Natl. Acad. Sci. U. S. A. 102 (2005) 10551–10556.

[69] B. Ramsay, B. Wiedenheft, M. Allen, G.H. Gauss, C.M. Lawrence, M. Young, T. Douglas, Dps-like protein from the hyperthermophilic archaeon Pyrococcus furiosus, J. Inorg. Biochem. 100 (2006) 1061–1068.

[70] G.H. Gauss, P. Benas, B. Wiedenheft, M. Young, T. Douglas, C.M. Lawrence, Structure of the DPS-like protein from Sulfolobus solfataricus reveals a bacterioferritin-like dimetal binding site within a DPS-like dodecameric assembly, Biochemistry 45 (2006) 10815–10827.

[71] T. Granier, B.L. d'Estaintot, B. Gallois, J.M. Chevalier, G. Precigoux, P. Santambrogio, P. Arosio, Structural description of the active sites of mouse L-chain ferritin at 1.2 Å resolution, J. Biol. Inorg. Chem. 8 (2003) 105–111.

[72] P.D. Hempstead, A.J. Hudson, P.J. Artymiuk, S.C. Andrews, M.J. Banfield, J.R. Guest, P.M. Harrison, Direct observation of the iron-binding sites in a ferritin, FEBS Lett. 350 (1994) 258–262.

[73] A. Treffry, Z.W. Zhao, M.A. Quail, J.R. Guest, P.M. Harrison, How the presence of three iron binding sites affects the iron storage function of the ferritin (EcFtnA) of Escherichia coli, FEBS Lett. 432 (1998) 213–218.

[74] G.C. Ford, P.M. Harrison, D.W. Rice, J.M.A. Smith, A. Treffry, J.L. White, J. Yariv, Ferritin—design and formation of an iron-storage molecule, Philos. Trans. R. Soc. Lond. B Biol. Sci. 304 (1984) 551–565.

[75] K.M. Towe, W.F. Bradley, Mineralogical constitution of colloidal hydrous ferric oxides, J. Colloid Interface Sci. 24 (1967) 384–392.

[76] F.M. Michel, L. Ehm, S.M. Antao, P.L. Lee, P.J. Chupas, G. Liu, D.R. Strongin, M.A.A. Schoonen, B.L. Phillips, J.B. Parise, The structure of ferrihydrite, a nanocrystalline material, Science 316 (2007) 1726–1729.

[77] P.M. Harrison, F.A. Fischbach, T.G. Hoy, G.H. Haggis, Ferric oxyhydroxide core of ferritin, Nature 216 (1967) 1188–1190.

[78] W.H. Massover, J.M. Cowley, Ultrastructure of ferritin macromolecules—lattice structure of core crystallites, Proc. Natl. Acad. Sci. U. S. A. 70 (1973) 3847–3851.

[79] N. Galvez, B. Fernandez, P. Sanchez, R. Cuesta, M. Ceolin, M. Clemente-Leon, S. Trasobares, M. Lopez-Haro, J.J. Calvino, O. Stephan, J.M. Dominguez-Vera, Comparative structural and chemical studies of ferritin cores with gradual removal of their iron contents, J. Am. Chem. Soc. 130 (2008) 8062–8068.

[80] G.R. Moore, S. Mann, J.V. Bannister, Isolation and Properties of the complex nonheme-iron-containing cytochrome b_{557} (bacterioferritin) from Pseudomonas aeruginosa, J. Inorg. Biochem. 28 (1986) 329–336.

[81] J.S. Rohrer, Q.T. Islam, G.D. Watt, D.E. Sayers, E.C. Theil, Iron environment in ferritin with large amounts of phosphate, from Azotobacter vinelandii and horse spleen, analyzed using extended X-ray absorption fine-structure (EXAFS), Biochemistry 29 (1990) 259–264.

[82] P. Doig, J.W. Austin, T.J. Trust, The Helicobacter pylori 19.6-kilodalton protein is an iron-containing protein resembling ferritin, J. Bacteriol. 175 (1993) 557–560.

[83] S. Baaghil, A.J. Thomson, G.R. Moore, N.E. Le Brun, Studies of copper(II)-binding to bacterioferritin and its effect on iron(II) oxidation, J. Chem. Soc.-Dalton Trans. (2002) 811–818.

[84] H. Aitken-Rogers, C. Singleton, A. Lewin, A. Taylor-Gee, G.R. Moore, N.E. Le Brun, Effect of phosphate on bacterioferritin-catalysed iron(II) oxidation, J. Biol. Inorg. Chem. 9 (2004) 161–170.

[85] T.G. St Pierre, S.H. Bell, D.P.E. Dickson, S. Mann, J. Webb, G.R. Moore, R.J.P. Williams, Mössbauer spectroscopic studies of the cores of human, limpet and bacterial ferritins, Biochim. Biophys. Acta 870 (1986) 127–134.

[86] M.P. Weir, T.J. Peters, J.F. Gibson, Electron spin resonance studies of splenic ferritin and hemosiderin, Biochim. Biophys. Acta 828 (1985) 298–305.

[87] N. Deighton, A. Aburaqabah, I.J. Rowland, M.C.R. Symons, T.J. Peters, R.J. Ward, Electron paramagnetic resonance studies of a range of ferritins and haemosiderins, J. Chem. Soc.-Faraday Trans. 87 (1991) 3193–3197.

[88] N.E. Le Brun, G.R. Moore, A.J. Thomson, Magnetic circular dichroism spectroscopy of the iron cores of ferritin and bacterioferritin, Mol. Phys. 85 (1995) 1061–1068.

[89] S. Mann, J.M. Williams, A. Treffry, P.M. Harrison, Reconstituted and native iron-cores of bacterioferritin and ferritin, J. Mol. Biol. 198 (1987) 405–416.

[90] N.M.K. Reid, D.P.E. Dickson, C. Greenwood, A. Thompson, F.H.A. Kadir, G.R. Moore, Evidence for Mössbauer spectroscopy for different forms of iron core in Pseudomonas aeruginosa bacterial ferritin, Biochem. J. 272 (1990) 263–264.

[91] G.D. Watt, R.B. Frankel, G.C. Papaefthymiou, K. Spartalian, E.I. Stiefel, Redox properties and Mössbauer spectroscopy of Azotobacter vinelandii Bacterioferritin, Biochemistry 25 (1986) 4330–4336.

[92] S. Levi, A. Luzzago, G. Cesareni, A. Cozzi, F. Franceschinelli, A. Albertini, P. Arosio, Mechanism of ferritin iron uptake-activity of the H-chain and deletion mapping of the ferro-oxidase site—a study of iron uptake and ferro-oxidase activity of human-liver, recombinant H-chain ferritins, and of 2 H-chain deletion mutants, J. Biol. Chem. 263 (1988) 18086–18092.

[93] G.H. Zhao, F. Bou-Abdallah, P. Arosio, S. Levi, C. Janus-Chandler, N.D. Chasteen, Multiple pathways for mineral core formation in mammalian apoferritin. The role of hydrogen peroxide, Biochemistry 42 (2003) 3142–3150.

[94] G.N.L. Jameson, W. Jin, C. Krebs, A.S. Perreira, P. Tavares, X.F. Liu, E.C. Theil, B.H. Huynh, Stoichiometric production of hydrogen peroxide and parallel formation of ferric multimers through decay of the diferric-peroxo complex, the first detectable intermediate in ferritin mineralization, Biochemistry 41 (2002) 13435–13443.

[95] G.S. Waldo, E.C. Theil, Formation of iron(III)-tyrosinate is the fastest reaction observed in ferritin, Biochemistry 32 (1993) 13262–13269.

[96] X.K. Yang, Y. Chen-Barrett, P. Arosio, N.D. Chasteen, Reaction paths of iron oxidation and hydrolysis in horse spleen and recombinant human ferritins, Biochemistry 37 (1998) 9743–9750.

[97] F. Bou-Abdallah, G.H. Zhao, H.R. Mayne, P. Arosio, N.D. Chasteen, Origin of the unusual kinetics of iron deposition in human H-chain ferritin, J. Am. Chem. Soc. 127 (2005) 3885–3893.

[98] B. Xu, N.D. Chasteen, Iron oxidation chemistry in ferritin—increasing Fe/O_2 Stoichiometry during core formation, J. Biol. Chem. 266 (1991) 19965–19970.

[99] I.G. Macara, P.M. Harrison, T.G. Hoy, Formation of ferritin from apoferritin—kinetics and mechanism of iron uptake, Biochem. J. 126 (1972) 151 -&.

[100] I.G. Macara, T.G. Hoy, P.M. Harrison, Formation of ferritin from apoferritin—catalytic action of apoferritin, Biochem. J. 135 (1973) 343–348.

[101] N.E. Le Brun, S.C. Andrews, J.R. Guest, P.M. Harrison, G.R. Moore, A.J. Thomson, Identification of the ferroxidase centre of Escherichia coli bacterioferritin, Biochem. J. 312 (1995) 385–392.

[102] F. Bou-Abdallah, A.C. Lewin, N.E. Le Brun, G.R. Moore, N.D. Chasteen, Iron detoxification properties of Escherichia coli bacterioferritin—attenuation of oxyradical chemistry, J. Biol. Chem. 277 (2002) 37064–37069.

[103] S. Baaghil, A. Lewin, G.R. Moore, N.E. Le Brun, Core formation in Escherichia coli bacterioferritin requires a functional ferroxidase center, Biochemistry 42 (2003) 14047–14056.

[104] T.L. Lawson, A. Crow, A. Lewin, S. Yasmin, G.R. Moore, N.E. Le Brun, Monitoring the iron status of the ferroxidase center of Escherichia coli bacterioferritin using fluorescence spectroscopy, Biochemistry 48 (2009) 9031–9039.

[105] G.D. Watt, R.B. Frankel, D. Jacobs, H.Q. Huang, Fe^{2+} and phosphate interactions in bacterial ferritin from Azotobacter vinelandii, Biochemistry 31 (1992) 5672–5679.

[106] E.R. Bauminger, A. Treffry, M.A. Quail, Z.W. Zhao, I. Nowik, P.M. Harrison, Metal binding at the active centre of the ferritin of Escherichia coli (EcFtnA). A Mössbauer spectroscopic study, Inorg. Chim. Acta 297 (2000) 171–180.

[107] Z.W. Zhao, A. Treffry, M.A. Quail, J.R. Guest, P.M. Harrison, Catalytic iron(II) oxidation in the non-haem ferritin of Escherichia coli: the early intermediate is not an iron tyrosinate, J. Chem. Soc. Dalton Trans. (1997) 3977–3978.

[108] F. Bou-Abdallah, G.C. Papaefthymiou, D.M. Scheswohl, S.D. Stanga, P. Arosio, N.D. Chasteen, mu-1, 2-peroxobridged di-iron(III) dimer formation in human H-chain ferritin, Biochem. J. 364 (2002) 57–63.

[109] K.H. Ebrahimi, P.L. Hagedoorn, J.A. Jongejan, W.R. Hagen, Catalysis of iron core formation in Pyrococcus furiosus ferritin, J. Biol. Inorg. Chem. 14 (2009) 1265–1274.

[110] J. Tatur, W.R. Hagen, The dinuclear iron-oxo ferroxidase center of Pyrococcus furiosus ferritin is a stable prosthetic group with unexpectedly high reduction potentials, FEBS Lett. 579 (2005) 4729–4732.

[111] J.D. Thompson, D.G. Higgins, T.J. Gibson, CLUSTAL W: improving the sensitivity of progressive multiple sequence alignment through sequence weighting, position-specific gap penalties and weight matrix choice, Nucl. Acids Res. 22 (1994) 4673–4680.

[112] K.B. Nicholas, H.B. Nicholas Jr., Genedoc: A tool for editing and annotating multiple sequence alignments, distributed by the authors, 1997.

[113] W.L. DeLano, The PyMOL Molecular Graphics System, DeLano Scientific, San Carlos, USA, 2002.